THE MINISTRY OF NATIONAL INFRASTRUCTURES
GEOLOGICAL SURVEY OF ISRAEL

An integrative approach for the study of surface sandy soils in the Galilee coastal plain

Alexander Tsatskin, Amir Sandler, Naomi Porat

Report GSI/26/2011 Jerusalem, October 2011

THE MINISTRY OF NATIONAL INFRASTRUCTURES
GEOLOGICAL SURVEY OF ISRAEL

An integrative approach for the study of surface sandy soils in the Galilee coastal plain

Alexander Tsatskin[1], Amir Sandler[2], Naomi Porat[2]

[1] Zinman Institute of Archaeology, University of Haifa

[2] Geological Survey of Israel

Report GSI/X/11 Jerusalem, October 2011

ABSTRACT

Surface hamra soils and related soils were studied in the southern part of the Evron kurkar ridge, between Akko and Lohamei HaGeta'ot. The study aimed, for the first time in the Galilee coastal plain to characterize properties and genesis of soils under the control of numerical dating. For these goals we applied a variety of pedological and geological methods that included: trench digging, field survey and description, micromorphology, grain size, $CaCO_3$ and SOC analyses, magnetic properties, clay fraction mineralogy, OSL and ^{14}C dating.

The active soils of the eastern slope of the Evron kurkar ridge at Shamerat, have redness and magnetic susceptibility values typical for hamra soils elsewhere. In addition, we found for the first time, widespread polygenetic hamra/husmas soils that probably inherited specific multi-phase calcareous nodules from earlier stages of soil development. The soils are developed on 2-3 m leached yellow-grayish sand which was dated by OSL to >~250 ka. Red-colored and magnetically enhanced hamra soils are also strongly enriched with 10-12 cm mole holes (bioturbation by rodents) and septaric carbonate nodules; they show distinct developed birefringence fabric ("aged clay") in thin sections and domination of smectitic illite-smectite in the clay fraction.

Adjacent but closely spaced hamra soils, mainly on the top of the ridge, show lesser redness values, do not have calcitic nodules, and locally have illitic composition of the illite-smectite. These soils were formed on Holocene sandy parent materials of 6 to 3 ka age that has been apparently blown off the Haifa Bay shore.

Sandy grayish vertic soil is found on the eastern slope of the Evron ridge either at the subsurface, below the Holocene hamra, or exposed as an active agricultural soil. The parent material of the vertic soil is assumed to have accumulated during the last glacial. The vertic soils are found on top of a red hamra/husmas soil with well-developed calcic horizon. The parent material of the hamra/husmas soil cannot be younger than ~200 ky. Further studies are needed to validate the assumption that the vertic soil fills up the gap between the formation of the strongly-developed, ancient-yet-nearly-exposed, hamra/husmas soils and the less developed Holocene hamra soils.

1. INTRODUCTION

Surface hamra soils in the Galilee coastal plain are restricted to the Evron ridge (Figs 1 and 2). The formation and development of hamra and related soils in the Galilee coastal plain are known much less than in the central part of the Israeli coastal plain. Hamra soils are genetically related to coastal sand dunes and are a product of pedogenic reworking of sandy materials under conditions of persistent deposition of eolian fine-grained dust (Dan et al., 2007; Singer, 2007). Supply of quartz sand by marine currents from the Nile delta to the Israeli coast is a continuous process, albeit with possible present-day disruptions due to the Aswan dam (Zviely et al., 2009). The Galilee coastal plain, situated to the north of the Ahihud Fault, is a unique segment of the Israeli coastal plain as it currently lacks Nilotic quartz sand supply because the Haifa bay serves as a natural depositional sink at the northern end of the Nile cell (Almagor, 2005). The Galilee coastal plain sediment is composed of coarse carbonate grains, locally called *zifzif* (Emery and Neev, 1960; see also review in Almagor, 2005). However, hamra and sandy soils have been earlier reported and mapped in this region on top of the Evron ridge (Avnimelech, 1943; Dan and Raz, 1970; Ministry of Agriculture, Soil associations Map 1:50,000), but have not been systematically studied. Since the 1970s, buried hamra paleosols were studied in the Evron ridge in relation to their prehistoric context (Gilead and Ronen, 1977; Ronen, 1991; Tchernov et al., 1994). Later, Sivan (1996) used paleosols to create a regional stratigraphic scheme, albeit without application of absolute dating techniques. The southern part of the Evron ridge is built of kurkar (calcite cemented sandstone) overlain by non-cemented sand, which is either a weathering product of the kurkar or accumulation of wind blown sand inland from the Haifa Bay (Almagor, 2005; Zvieli et al., 2007).

The current study focuses on surface sandy soils in the southern part of the Evron ridge area. Associated paleosols were studied, where encountered. The study aims at characterizing soils age, properties and genesis in order to shed light on the relations between modern environmental conditions and soil processes and to clarify the potential role of surface soils in the Quaternary stratigraphy of the area. For these goals we applied integration of pedological, geological and geochronological techniques in the study area, where such an interdisciplinary approach has not yet been taken.

2. CHRONOSTRATIGRAPHIC AND PEDOLOGICAL BACKGROUND

The basic knowledge of hamra soils genesis and spatial variability along the coastal landforms was initially obtained in the central and southern coastal plain (Dan et al., 1969;

Dan and Koyumdjiski, 1979). Hamra soils were found in spatial toposequences, or catenas, along with adjacent lowland clayey soils, termed grumusols (Dan et al., 1969; Yaalon and Kalmar, 1978; Dan, 1983), which are equivalent to vertisols in the international soil classification schemes. The fine fraction in hamra soils, as well as in other soils in the East Mediterranean region, has been suggested to mainly derive by long-distance transported dust from the Sahara and Arabia deserts (Yaalon, 1997).

Luminescence dating of kurkar outcrops exposed along the coastal cliffs of the Mediterranean Sea between Haifa and Tel-Aviv (Frechen et al., 2004; Sivan & Porat, 2004) suggested that hamra soil forming processes operated over several 10^3 years, i.e. much longer than previously thought (Porat et al., 2004). Gvirtzman and Wieder (2001) refined the chronostratigraphic division of the Late Pleistocene pedocomplex, termed Netanya hamra, and correlated the terrestrial environmental changes with global marine oxygen isotope stages from stage 4 onward. The archaeological findings of Mousterian (~40 ka ago) and Epipalaeolithic (~19-15 ka ago) prehistoric tools within the Netanya pedocomplex at Nahal Hadera outlet, first reported by Tsatskin et al. (2008), are in good agreement with the estimates of the duration of hamra formation by Porat et al (2004).

Numerical dating of paleo-hamra-kurkar sequences were performed in the Galilee coastal plain only in the Evron quarry and the nearby Ness Amim quarry. At both locations the infra-red stimulated luminescence (IRSL) ages of alkali feldspars were in the range of 330 to 630 ka (Porat and Ronen, 2002; Porat, unpublished data), i.e. at the time limit of the IRSL method, which suggests that true ages may be even older. A recent study of the Haifa Bay subsurface provided novel data on long sequences of kurkar beds and hamra paleosols alternating with marine clays and sand layers (Avnaim-Katav, 2011). Cosmogenic radionuclide dating and paleomagnetic data from core samples indicated that the oldest hamra in the sequence was formed not earlier than ca. 1.2 Ma, while optically stimulated luminescence (OSL) ages of hamra at the upper part of the cores were 120-160 ka (Avnaim-Katav, 2011). The relevant question is then whether nearby surface hamra soils of the Galilee coastal plain are analogous to the adjacent ancient hamra paleosols in the Haifa Bay subsurface. This question is critical in understanding the regional climate change and the history of marine transgressions during the Quaternary.

Soil micromorphology, which is a study of petrographic thin sections of undisturbed soil samples, is a potent tool for deciphering formative processes in such complex natural systems (Stoops et al, 2010). For example, micromophology allowed Wieder and Yaalon (1974) to demonstrate the dependence of calcite accumulation in Israeli soils upon the fabric

of soil materials and to describe some pathways of their transformation over time. The authors distinguished calcite nodules formed in situ (orthic) from disturbed or transported nodules (disorthic and allothic). In carbonate-free soils like hamras, there is a need to focus on other relevant components of soil microfabric, e.g. illuviation coatings, as an efficient indicator of soil evolution (Fedoroff et al., 2010). However, a more recent study (Tsatskin and Ronen, 1999) showed that coatings on sand grains were not necessarily the result of clay translocation but could result from extreme events such as desiccation, surface crusting and erosion of broken crusts to lower positions.

Well-developed hamra soils have a bright red color 5YR and higher and very low to no carbonate content. As the sandy parent material is highly permeable and leaching is intensive, the clay minerals are easily transformed and iron oxides are released and accumulate as discrete phases (Singer, 2007). A recent research on quantitative soil clay mineralogy (Sandler, 2009) suggested that pedogenic neoformation of clay minerals is more pronounced in hamra soils than in other Mediterranean soils and might serve as an indicator for soil maturity. Pronounced changes in clay minerals in hamra soils, relative to settled dust clays, are manifested by decrease of smectite and illite-smectite phases and increase of kaolinite and illite, whereas vertisols are enriched with smectitic phase and depleted with kaolinite and illite (Sandler et al., 2009).

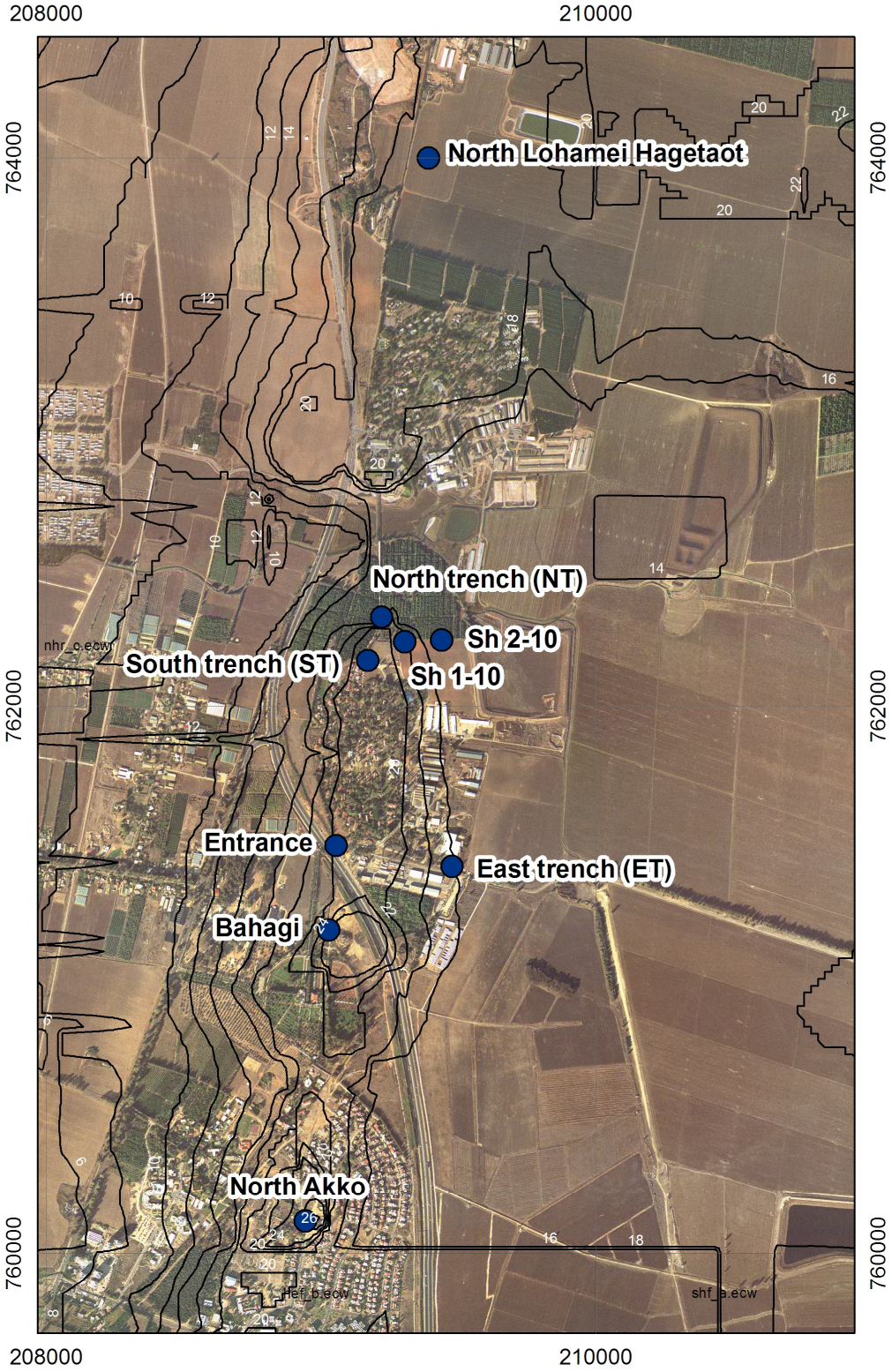

Figure 1. Location map of the study area showing the key sites as detailed in Table 1 (the 2 m interval contours were prepared on the basis of the digital shaded relief map of Israel 1:500,000 by Hall and Calvo (from http://www.cybaes.org/archive/downloads/Hall2005/PlXI.pdf)

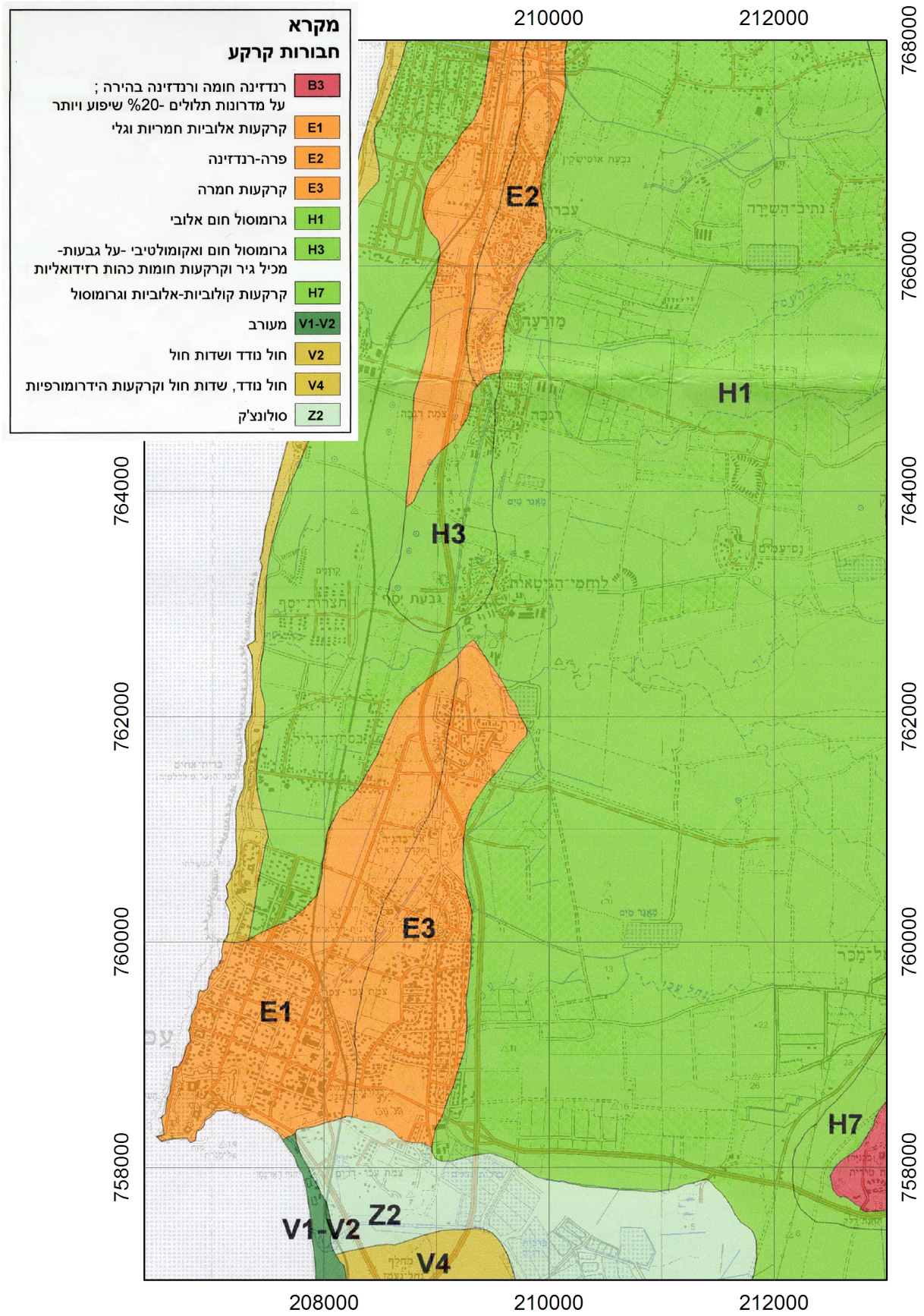

Figure 2. Soil associations map of the Galilee coastal plain (Ministry of Agriculture, originally 1: 50,000). E3 = Hamra soils.

3. STUDY AREA AND SECTIONS

The Evron ridge is located ca. 1 - 2 km eastward from, and parallel to, the coastline from Akko northward. It is the eastern of the two kurkar ridges exposed in the Galilee coastal plain; the western one is located at or near the coastline. The Evron ridge rises to 5 - 10 m above the surrounding flatland and reaches the maximum elevation of 40 m above sea level near Evron (Almagor, 2005). Many of the settlements of the Galilee coastal plain are located on the Evron ridge, which is intensely utilized either by construction or as agricultural fields. Flatlands occupied by vertisols are located between the ridge and the western foothills of the Galilee Mountains. The Evron ridge was suggested to form during MIS 6, around 150-200 ka ago (Sivan, 1996), but later IRSL dating results (Porat and Ronen, 2002; Porat, unpublished) enabled to assigned its age to at least 600 ky.

The area between Tel Akko and Lohamei HaGeta'ot (Fig. 1) was thoroughly surveyed in order to find suitable sites for pedologic/geologic investigation. Systematic sampling was carried out mainly in and around kibbutz Shamerat. Two ~3 m deep trenches were dug by a back-hoe excavator for the purpose of the current study and allowed us to study catenary changes along the eastern leeward slope of the Evron ridge; trench SH-1-10 is close to the top and trench SH-2-10 is on the middle/lower part of the slope. Five other shallower trenches, dug by various authorities, were also used for this study (Fig. 1); four water pipes trenches ~1.8 m deep and a wiring trench ~1.2 m deep. A few natural and artificial sections were sampled as well. Overall, nine sites (Table 1, Fig. 1) were described and analyzed, including ~ 40 samples for particle size, 20 samples for micromorphology, 11 samples for OSL dating, and 3 samples for ^{14}C AMS dating. Each site is described in detail, to include all data gathered, followed by a summary of each of the main analytical method for all sites.

Table 1. Sites studied

Site No.	Name	Location	Coordinates	Geomorphic position, field definition	Depth, special features
1	Sh 1-10	Shamerat	209353/762265	Upper slope, red hamra	3.5 m, kurkar blocks
2	Sh 2-10	Shamerat	209441/762265	Middle slope, brown hamra	3 m, kurkar blocks
3	East trench (ET)	Shamerat	209588/761441	Toeslope, hamra upon vertic paleosol	1.95 m, mixed calcrete with kurkar
4	Bahagi	Bahagi memorial	208905/761480	West slope, hamra	1.2 m, ceramic sherds
5	North trench (NT)	Shamerat	209220/762325	Lower slope, hamra	1.55 m
6	South trench (ST)	Shamerat	209169/762167	Upper slope, hamra	1.25 m
7	Entrance	Shamerat	209054/761490	Upper west slope, hamra	2.0 m
8	North Akko	North Akko	208941/760118	Various sands and hamra	~0.1-1.8 m
9	North Lohamei HaGeta'ot (NLH)	Between Lohamei HaGeta'ot and Regba	209305/764005	West upper slope, vertic soil (exhumed paleosol)	1.8

4. METHODS

Field methods: Soils and soil substrates were described in the field according to Dan and Koyumdjiski (1979). Detailed description and sampling were performed on the two ~3 m deep trenches and on two of the other trenches at the time of their excavation. Some trenches were dug deeper by hand in order to reach deeper levels. Samples were generally taken in duplicates: for thin sections and for other analyses.

An archaeological survey, which intended to locate both prehistoric flint artifacts and historic ceramic sherds with regard to stratigraphic layers, resulted in just a few findings.

Sample processing: Samples were dried at room temperature, gently crushed and sieved through a 2 mm sieve. The <2 mm fraction was used for all types of analyses, excluding thin section petrography. A portion of this fraction was grinded and the powder was used for $CaCO_3$ and organic carbon (TOC) determinations in selected samples. The latter is presented here as soil organic carbon (SOC).

$CaCO_3$ concentration was determined by a calcimeter on 0.5 g of a powder. The limit of detection was 0.5%.

Soil organic carbon (SOC) was determined by wet oxidation of 1 g sample with potassium dichromate, followed by titration with ferrous ammonium sulfate. The limit of detection is 0.1%.

Grain size analysis determined the sand (63 - 2000 μm), silt (2 - 63 μm) and clay (<2 μm) fractions as follows: 20 g were put with water in a plastic tube that was mechanically rotated for six hours. The tube was treated for a few minutes in an ultrasonic (US) bath and the sample was sieved through a 63 μm sieve. The sand fraction was dried and weighted and the fine fraction was put into cylinders of 2 liter volume. The clay fraction was decanted according to Stokes's law repeatedly using US bath and sodium hexametaphosphate (calgon) until complete removal. The silt fraction left was dried and weighted and the clay fraction weight was calculated by subtraction.

Color values were assessed by the Munsell color chart and measured by spectrocolorimeter Specbos 4000 (JETI, Jena).

Magnetic properties, including low-field magnetic susceptibility and susceptibility difference, were measured by Bartington MS2 magnetic susceptibility meter (Oxford, England).

Thin sections were prepared after impregnation of undisturbed blocks by polyester resin, slicing and polishing down to 0.03 mm. Thin sections were analyzed with a polarized light microscope Olympus-2, described according to Stoops (2003) and photographed.

Clay fraction mineralogy: The clay fraction for mineralogical determination was extracted from original samples as follows: About 10 g were rotated with water for 6 hours followed by repeated addition of buffered acetic acid (pH = 4.8) until complete dissolution of salts and carbonates. The clay fraction was decanted from a stable thin suspension according to Stokes law after repeated washing and a 2 minutes US treatment. The clay suspension was saturated with strontium and pipetted onto glass slides. Three XRD runs were carried out: after air-drying, glycolation (at least 8h at 60ºC and cooling overnight), and heating to 550ºC for 2 hours. A Philips X-ray diffractometer (1730/1710) was operated with 40 kV and 30 mA, CuKα radiation. Semi-quantitative clay composition was calculated from the peak areas of illite-smectite (IS), kaolinite and illite, and the expandability of the IS was explored by the saddle value (modified after Sandler and Herut, 2000). Kaolinite-smectite (KaS) mixed-layer was identified by the expansion of a shoulder on the lower angle side of kaolinite after glycolation. KaS and goethite reflections were very small relative to IS and kaolinite and were not quantified.

OSL dating: To prevent any exposure to sunlight, samples were collected under a dark sheet from holes drilled horizontally into the sections, placed immediately into light-tight bags and processed at the laboratory of the Geological Survey of Israel (GSI) under suitable lighting. An additional sample was collected from each location for dose rate determinations. Quartz was extracted and purified using standard laboratory procedures (Porat, 2007). Equivalent dose (D_e) values were determined using the OSL or the TT-OSL signals and the single aliquot regenerative dose (SAR) protocol (Murray and Wintle, 2000; Wintle and Murray, 2006, Porat et al., 2009). The equivalent doses are the averages of 5-7 individual aliquots measured for the old, saturated samples, and 13-19 aliquots measured for the younger samples (Table 3). Dose rates were calculated from the concentrations of the radioactive elements, U, Th and K, measured by ICP-MS, and burial depths. Time-averaged water contents were estimated at 10±3%, taking into account seasonal variations.

Radiocarbon dating: The ^{14}C AMS dating of soil organic carbon was carried out in the Poznan Radiocarbon Laboratory (Poland), which is equipped with Accelerator Mass-Spectrometer 1.5 SDH-Pelletron Model "Compact Carbon AMS" (National Electrostatics Corporation, Middleton, USA). The ^{14}C activity of the insoluble fraction of organic carbon, termed humin, was measured. For the details of the procedures used see the http://radiocarbon.pl website. The dates obtained are uncalibrated.

5. RESULTS

5.1 Soil sequences on the eastward ridge slope

A survey for archeological findings resulted in a few surface artifacts of a pseudo-Levallois point and a broken Levallois scraper, presumably related to Mousterian culture (50-200 ka ago) (diagnosed by Prof. Avraham Ronen, personal communication).

Surface soils of Shamerat at Sh 1-10 and Sh 2-10 sites were found on the upper part and on the middle/lower part, respectively, of a gentle slope of ~10° angle, upon relatively thick sand substrate. Ages and other key characteristics of both sites are described below and summarized in Tables 2 and 3.

Sh 1-10

$A_{p\,(k)}$ horizon (ploughed), 0-0.2 m: 5YR 4/6 yellow red sandy loam, compacted, porous, abundant rootlets, strongly finely mottled due to bioturbation by insects and earthworms (?); the mottles are of both reddish and brown hue; rare small, up to 4 mm, soft $CaCO_3$ nodules; gradual transition.

Figure 3. Surface soil morphology (a) at site 1-10, on Shamerat upper eastern slope, (b) at site 2-10, on Shamrat lower eastern slope.

AB_k horizon, 0.2-0.6 m: mottled and strongly bioturbated by krotovinas (mole holes) ~0.6-0.8 cm in diameter, partly welded; red 2.5YR 3/6 mottles are superimposed upon yellow red 5YR 4/6 and strongly brown mottles (patches); less firm, poorly structured; contains scattered strongly developed, hard septaric nodules, 2-4 cm in size (Fig. 4); gradual transition. OSL age of a sample taken from the transition zone is >256±72 ky.

BC_k horizon, 0.6-1.2 m: 5YR 5/6 yellowish-red loamy sand, less firm, heterogeneous in color due to overwhelming krotovinas, some reaching 8-10 cm in diameter; scattered septaric nodules similar to above; gradual transition.

C horizon, 1.2-1.3 m: strong brown 7.5 YR 6/8 sand, calcareous-free; sharp contact. From 1.3 m to ~3 m depth grayish sand with scattered large krotovinas up to 12 cm in diameter, all filled with brown loam grading to grayish sand with 10YR 6/6 color. This sand grades downward to a lighter color sand, which contains blocks of strongly $CaCO_3$ cemented sand (apparently, relict blocks of kurkar). OSL age of a sample taken from 1.5 m depth is >276±90. On the northern side of the trench the contact between the grayish and the light-colored sands appears as funnel-like structure measuring 1.5 m x 0.8 m with blurred

boundaries. This structure is not reflected in any way on horizonation and soil properties. The trench originally reached ~ 4 m depth.

Figure 4. Large septaric nodule from site Sh-1-10, 0.4 m depth.

Except for the top 1 cm, the amount of $CaCO_3$ in the <2 mm fraction is negligible (< 0.8%) all along the section (Table 2), despite the appreciable quantity of large carbonate nodules within the A and AB soil horizons. The latter show a septaric structure and are rather unusual in hamra soils. The topsoil SOC concentration is 0.29%, whereas that of all other samples is below the detection limit (0.1%).

The grain size distribution exhibits clear differentiation of the sequence into an upper unit, including the soil profile, and a lower unit of substrate sand below 1.32 m. The clay content within the soil profile is 11 to 18%, whereas the silt content varies between 0.3 to 3 %.

The digital color indices and magnetic susceptibility (Fig. 5) of the soil are higher than the underlying sand, which is characteristic for well-drained soils elsewhere (Evans, Heller, 2003). The χ values in the topsoil are 40 - 50x$10^{-8}$$m^3$$kg^{-1}$ and they gradually decrease down the profile to very low values of 5 - 10x$10^{-8}$$m^3$$kg^{-1}$. Two small spikes seen on the graph in Figure 5 at 1.3 and 1.75 m depth are associated with krotovinas, filled with red soil material from the A horizon, which may be either a current one or a former, no longer preserved one.

The a* values of redness vary along the profile from 14-15 units at 0.05 m depth to maximal value of ~20 units at ca. 0.3-0.4 m depth, which is in accord with redness by Munsell chart. Below 0.5 m depth the redness value decreases gradually reaching ~10-12 units at 1.7 m depth in brown sands, whereas below 2.4 m it drops sharply to ~ 2 units (white

sand). The lightness L* increases gradually with depth, approaching 80-90 units in the white sands. Positive b* values, a measure of yellowness (in case of soils, apparently brownness) increase with depth and show maximum values between 0.9 to 1.7 m.

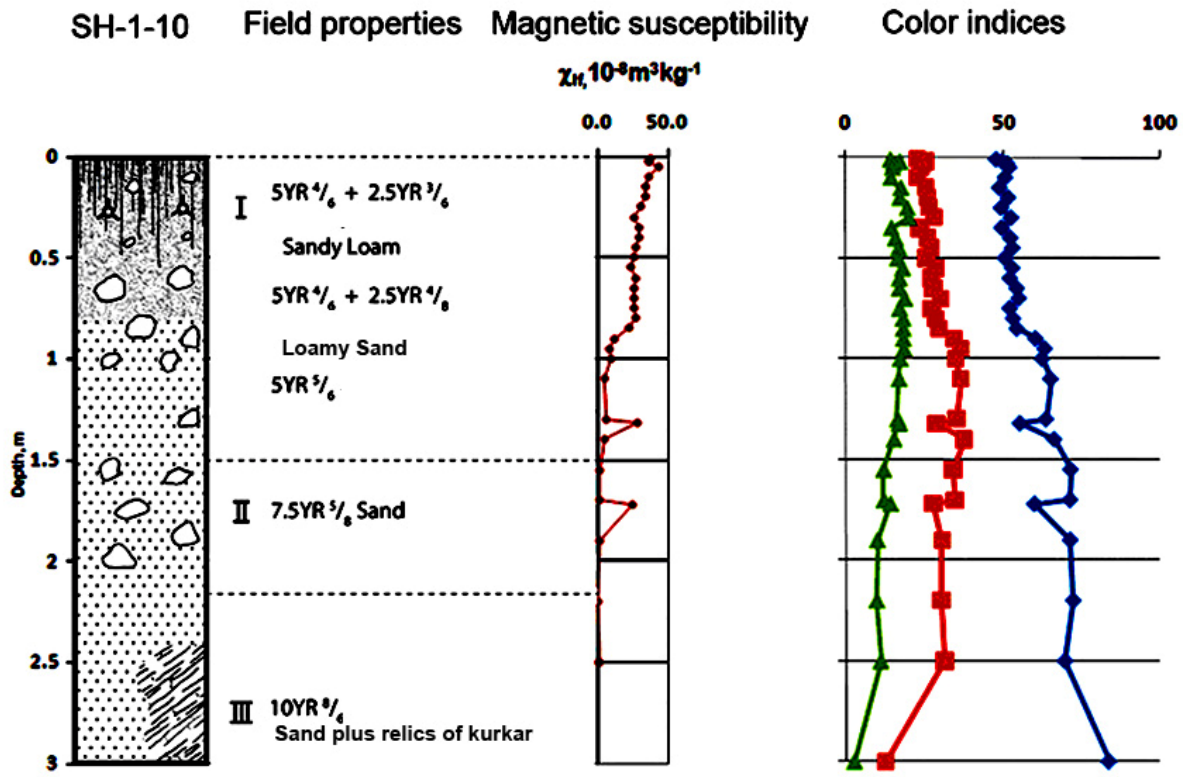

Figure 5. Color indices and magnetic properties of section Sh-1-10.

The clay fraction mineralogical composition exhibits only slight variation along the soil profile with dominance of IS (~65-80%) and minor kaolinite amount (~10-25%) (Fig. 16). Kaolinite amount is somewhat higher at the AB_k horizon and somewhat lower than the average at the topsoil. The saddle values are uniform (0.72-0.78), indicating a medium illitic content of the IS composition, which is higher than that of Galilee dust and lower than that of typical hamra soils. Illite, goethite and KaS are present in very low amounts (Table 4). The clay mineral assemblage differs from that of hamras in the subsurface of the Haifa Bay (Sandler et al., 2007) and from surface hamra in the Sharon (Sandler et al., 2009).

In sum, the field observations and the analytical data show that the surface soil in this sequence is strongly bioturbated hamra. However, the question of soil taxonomy is addressed in the discussion.

Sh 2-10

A_{pk} horizon, strongly varies in thickness from 0.02 cm in a western side to 0.4m in the southern side of the trench: strong brown 7.5YR 4/6 loam; poorly aggregated, feeble granular, massive, porous; abundant rootlets, mostly charred; feeble mottling probably due to bioturbation; ~ 1 cm in size worm/insect burrows; common soft $CaCO_3$ nodules with hard core, ca. 1 cm in size; gradual transition but in places a plough pan is observed.

AB_k horizon, ~0.2-0.8 m: yellow-red 5YR 4/6 to yellowish sandy loam; feeble blocky, rather firm; common ~ 1 cm in size earthworm burrows; common calcareous mottles and nodules with soft edge and a harder core, some nodules are of irregular shape; gradual transition.

BC_k horizon, 0.8-1.1 (1.5) m: reddish-yellowish 5YR 5/6 loamy sand to sand; less firm, heterogeneous in color due to abundant zones of whitish firm irregular $CaCO_3$ nodules, measuring 10x20 cm, apparently of secondary origin; some brown krotovinas of ~8 cm size; clear but irregular transition. The OSL age of a sample from 1.3m depth is >310±93.

C_k horizon, 15-3.0 m (visible): yellow sand in the upper part with calcareous impregnated soft zones and small, ~ 2-3 cm, dense nodules. Grayish sand and whitish sand with blocks of kurkar at about 2.5 – 3 m depth. The OSL age of a sample from 2.1m depth is >251±38.

Calcitic soft small nodules and hard shapeless, septaric nodules are more abundant than in the Sh 1-10 site, and so is the $CaCO_3$ amount in the <2 mm fraction, which reaches 5.5% at 25 cm depth . The SOC concentration at the upper part is also higher than at the Sh 1-10 site.

In terms of grain size distribution, the upper horizons contain 18 - 23% clay and 1 - 8% silt fraction. The sand fraction increases downward from 71% on top of the soil to 94% in parent material. In krotovina infilling at 0.75 m depth sand reaches 66% while clay fraction increases to 32%.

The a* values of redness is only half the values in the Sh 1-10 site, whereas the b* values of yellowness are substantially higher. This indicates that the soil here is browner, compared to the reddish color of the Sh-1-10 soil.

The clay fraction mineralogical composition (Fig. 16) is rather uniform along the soil profile with dominance of IS (~75-80%) and minor kaolinite amount (~15-20%). The amount of IS is somewhat higher and that of kaolinite lower than in the Sh 1-10 site. A significant difference is the lower saddle values (0.50-0.69 vs. 0.72-0.78), which indicates that Sh 2-10 profile has a substantially more smectitic composition of the IS. Illite and KaS are present in trace amounts or absent.

Both surface soil profiles seem basically similar and genetically related. The differences between them, manifested in larger abundance of $CaCO_3$ accumulation in Sh 2-10, enhanced fineness of the texture and higher smectitic composition of the IS phases, all indicate that the Sh-2-10 profile developed under restricted leaching due to its low geomorphic position. However, both soils formed on non-calcareous sands of the same age group, i.e. older than ~250 ky.

East trench (ET)

The ET site is a water pipes trench at the toe leeward (eastern) slope of the Evron ridge, a few hundred meters south of the Sh-1-10 and Sh-2-10 sites (Fig. 1). The properties and OSL dating results of the site are presented in Table 2. The ET sequence consists of three distinct pedostratigraphic layers (Fig. 6).

Figure 6. Comlex sequence of stratigraphy at the ET site.

1. The uppermost soil layer, 0-0.6 m: reddish brown 7.5YR 5/6 loose sand with grayish speckles (probably from bioturbation). This is an active surface soil which morphologically is similar to hamra, partially disturbed by anthropogenic activities; contains plant remnants

Table 2. Properties of soils
a. soils on the eastern ridge slope

Site	Horizon	Depth, m	Color Munsell	Texture, calcitic nodules, biofeatures	$CaCO_3$ %	TOC %	Sand %	Silt %	Clay %	Age ky OSL
Sh 1-10	$A_{p(k)}$	0.01	5YR 4/6	sandy loam, few tiny soft-dense nodules, bioturbation	2.0	0.29	83	1.9	15	
	AB_k	0.4	5YR 4/6 and 2.5YR 4/8	sandy loam, very few dense septaric nodules ~3 cm, mole holes	<0.8	<0.1	80	1.75	18	
	AB_k	0.6		sandy loam	<0.8	<0.1				>256±72
	BC_k	0.75		sandy loam	<0.8	<0.1	82	1.8	16	
	BC_k	0.95	5YR 5/6	sandy loam, carbonate nodules disappear, mole holes	<0.8	<0.1	79	2.8	18	
	C	1.32		loamy sand	<0.8	<0.1	88	1.25	11	
	C	1.5		loamy sand						>276±90
	C	1.9		sand	<0.8		96	0.45	3.6	
	C	3		sand	<0.8		97	0.3	2.7	
SH 2-10	A_{pk}	0.05	7.5YR 4/6	sandy clay loam	2.1	0.43	71	8	21	
	AB_k	0.25	5YR 4/6	sandy clay loam	5.5	0.13	75	1.7	23	
	AB_k	0.63	5YR 5/6	sandy clay loam			75	6	19	
	AB_k	0.75	7.5YR 5/6	sandy clay loam	3.3	<0.1	66	1.8	32	
	BC_k	1.1		sandy loam			81	1.0	18	
	BC_k	1.3		sandy loam						>310±93
	BC_k	1.6	10YR 6/6	loamy sand	<0.8	<0.1	85	0.8	14	
	C_k	1.87		sand	24	0.11	94	0.8	5.3	
		2.1		sand	14		92	0.9	7.1	>251±38
ET	layer 1	0.45	7.5YR 5/6	sandy clay loam, biotubation	<0.5		69	9	22	6.1±1.9
		0.5		sandy clay loam	<0.5		56	13	31	
	layer 2	1.3	10YR 3/3	sandy clay loam, prismatic structure, stiff						15±4
	layer 3	1.6	2.5YR 5/8	sandy clay loam with high amount of nodules	12.7		61	10	29	211±66; 195±45
		1.95		calcic horizon with sandy clay loam	-		-	-	-	215±58; 185±19

b. soils on the western ridge slope and additional sites

Site	Horizon	Depth m	Color Munsell	Texture, calcitic nodules, biofeatures	$CaCO_3$ %	SOC %	Sand %	Silt %	Clay %	Age ky OSL, ^{14}C
Bahagi	$A_{(p)}$	0.45	2.5YR 4/3	loamy sand covered by re-located sand			78	6	18	0.44±30 ^{14}C
	B1	0.73	7.5 YR 5/6	sandy clay loam, weathered ceramic sherds, tiny charcoal	<0.5	0.17	84	6	10	2.03±40 ^{14}C
	B2	0.92	7.5 YR 4/6	sandy loam, bioturbation	<0.5	0.11	76	4.1	20	3.0±0.5 OSL
	BC	1.05		sandy loam, bioturbation			71	6	23	
	BC	1.20	7.5YR 6/6	sandy loam, bioturbation	<0.5	0.1	70	7	23	3.59±70 ^{14}C
NT	Unit I, A_p	0.2	5YR 5/8	sandy clay loam	1.6		70	7	23	
	BC	0.38	5YR 5/6	loamy sand, bioturbation	<0.5		84	2.4	14	
	BC	0.64	5YR 5/8	sandy loam	<0.5		73	4	23	
	Unit II, B2	1.25	7.5YR 4/6	sandy loam	1.2		76	5	19	
ST	$AB_{p(k)}$	0.30	5YR 5/6	loamy sand, bioturbation	1.5		82	2.1	16	
	$BC1_{(k)}$	0.52	5YR 6/8	sand, bioturbation	1.3		87	1.3	12	
	$BC2_{(k)}$	0.77	5YR 5/8	sand, bioturbation	1.5		87	1.7	11	
	C	1.0	7.5YR 6/8	sand	1.3		92	1	7	
Entrance	B	1.75	5YR 5/8	loamy sand	1.2		87	1.4	12	
North Akko	AB	0.46	10YR 5/4	sand, covered by construction material	23		87	3.9	9	
	B	0.73	7.5YR 5/8	loamy sand	22		91	2.0	7	
	BC	1.26	2.5YR 8/4	loose sand	23		90	0.4	0.6	
	C	1.8	2.5YR 8/3	loose sand						
NLH	$Ap_{(k)}$	0.25		sandy clay loam, small nodules	<0.5	0.25	59	9	32	
	$B1_{(k)}$	0.80		sandy clay loam, nodules	<0.5	<0.1	56	8	36	102±20 OSL
	B2k	0.95		sandy clay loam, nodules	<0.5	<0.1	57	7	36	
	B2k	1.80		sandy loam, nodules	<0.5	<0.1	71	3.8	25	

near the surface and rootlets throughout; slightly bioturbated by mole holes filled with light-colored sand; gradual transition. The OSL age of a sample at 0.5m is 6.1±1.9 ka.

2. The middle soil layer, 0.6 – 1.35 m: brown gray 10YR 3/3 clayey fine sand, compacted, strongly vertically dissected to form prismatic structural units of up to 20-30 cm length with abundant slickensides; gradual transition from 1.35 m to 1.43 m. This soil layer is similar to vertisol (Yaalon and Kalmar, 1978) and a sample at 1.3 m is dated to 15±4 ka by OSL.

3. The lower layer, 1.43 – 1.95 m: a mixture of a hard cemented carbonate material of unidentified origin and strong red-brown 2.5YR 5/8 clay loam similar to hamra soil. This mixture could be either a soil developed on weathered kurkar or strongly developed carbonate nodules within a loamy hamra paleosol. The base of the layer was not reached. The OSL and TT-OSL ages of a sample at 1.6 m are 211±66 and 195±45, respectively. The OSL and TT-OSL ages of a sample at 1.95 m are 215±58 and 185±195, respectively.

The $CaCO_3$ content of the upper and middle layers was below the detection limit, whereas that of the lower calcitic red soil was 12.7%.

The grain size distribution in the three layers is characterized by relatively high clay and silt fractions content, with a maximum of 44% "silt plus clay" in the vertic sandy soil vs. 31% in the uppermost hamra.

The clay fraction mineralogical composition of the three layers is similar to that of Sh 2-10 site, but the saddle value of the two lower layers is as low as 0.45 (vertic paleosol) and 0.48 (the lowermost hamra mixed with carbonate). The low saddle values are clear indication of more smectitic composition of the IS mixed-layered mineral, which roughly corresponds to 25% illitic interlayers. Such a high smectitic composition was also found in a sandy vertisol at Bet Dagan (Sandler et al, 2009). Goethite was identified in the modern hamra and in the lower reddish paleosol and KaS was identified only in the upper hamra (Table 4).

5.2 Soil sequences on the westward slope and on top of the ridge

Bahagi

The section in the Bahagi site was studied in a wiring trench of 1.2 m depth where an artificial layer was laid upon the soil profile (Fig. 7, Tables 2 and 3).

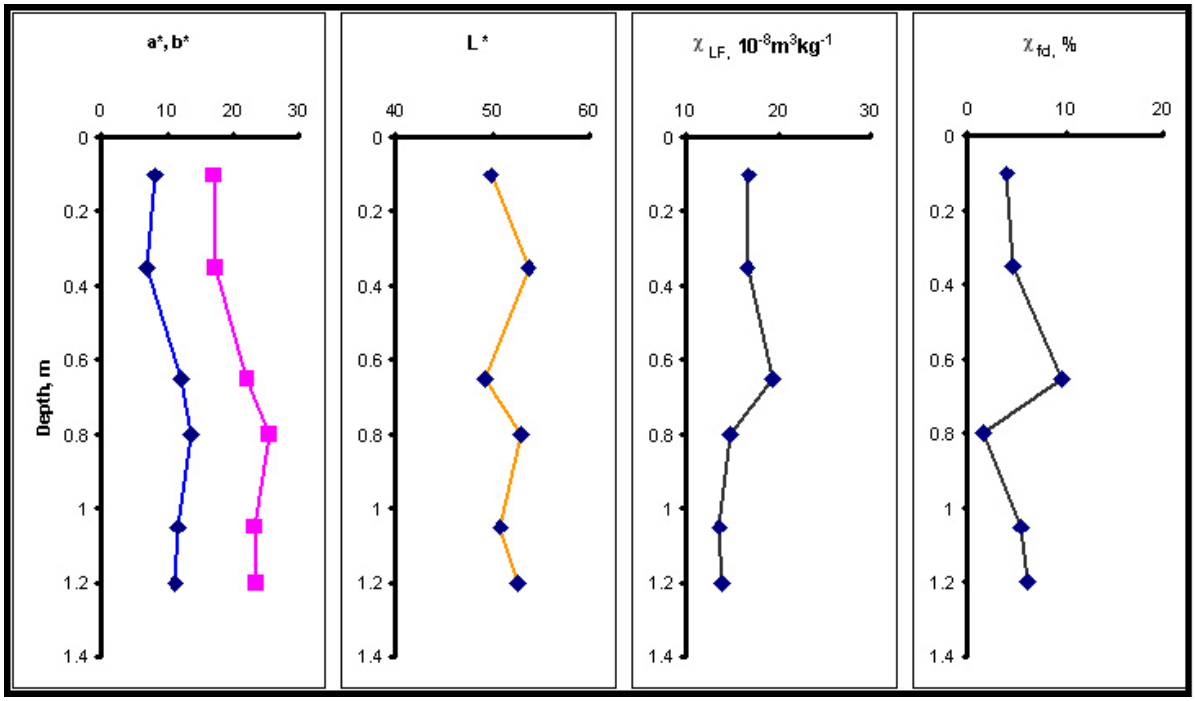

Figure 7. Surface soil morphology at Bahagi site.

I. A layer affected by current building activities, including external material, 0-0.25 m: grayish to dark yellowish-brown 10YR 4/6 fine sand; loose, soft, poorly aggregated, with some building stones; gradual transition.

II. Soil profile

$A_{(p)}$ horizon, 0.25 – 0.4(0.45) m: olive brown 2.5YR 4/3 loamy sand with rootlets; poorly observable plough pan forms the lower contact, inclined at ~5° relative to the modern surface, wavy lower transition. The horizon was dated by ^{14}C to ~400 years BP.

B1 horizon, 0.45-0.73 m: blurred brown 7.5 YR 5/6 sandy clay loam; compacted, vaguely blocky-prismatic, incipient slickensides; heterogeneous due to millimeter-scaled, tiny manganese nodules and coatings in rootlet vughs, charcoal pieces of less than 0.5 mm in size; contains weathered ceramic sherds, difficult to identify and date but possibly related to the Roman period (determination by Dr. Michael Aizenberg); gradual transition. The horizon was dated by ^{14}C to ~2,000 years BP, which agrees well with the archaeological findings.

B2 horizon, 0.73- 0.92 m: blurred brown 7.5 YR 4/6 sandy clay loam; prismatic, similar to above, but without coatings or slickensides; contains higher amount of fragmented ceramic materials, utterly unidentifiable; gradual transition. The horizon was dated by OSL to 3.0 ±0.5 ka, in agreement with the ^{14}C ages.

BC horizon, 0.92 to 1.20 m: yellowish 7.5YR 6/6 sandy clay loam; less compacted, bioturbated (worms, insects, roots), mottled; gradually becomes grayish downward. The horizon is dated by ^{14}C to ~3,500 years BP.

The $CaCO_3$ content of the three samples analyzed was <0.5%, as in most samples of the other sites. SOC decreased from 0.17% at the $A_{(p)}$ horizon to <0.1% at the BC horizon.

Grain size distribution shows a decrease of sand content from 84 % in the A_p horizon to 70 % in the lowermost BC horizon, accompanied by an increase in the clay content up to 23%. The silt content varies between 4.1 to 6.9 %, which is three times higher than in the Sh 1-10 and Sh 2-10 sites, but is about half of that in the ET site.

Color measurements show that maximal redness and yellowness is found at 0.85 m depth interval (upper B2 horizon) with a* and b* values of 13 and 25, respectively. The upper horizons and the parent material have lower a* and b* values. The a* value here is significantly lower than the reddest parts in the A horizon of the Sh 1-10 profile where a* reaches ~20 units. It is worth noting that the maximal values of magnetic susceptibility χ ($\sim 20 \times 10^{-8} m^3 kg^{-1}$) and of susceptibility difference χ_{fd} (~10%) are found at 0.65 m depth and do not coincide with maximal redness (Fig. 8). Here, Roman sherds were found and soil organic material yielded a ^{14}C age of ~2,000 years BP.

Measurements of magnetic parameters in soils demonstrated that larger χ_{fd} values result from higher concentration of very small pedogenic magnetite particles and are found in surface soil horizons (e.g. Evans and Heller, 2003). Hence, we may suggest that the magnetic susceptibility peak at ~0.65 m depth marks the ancient surface of a soil about two millennia ago, at a time of settlement and/or agricultural activity. Accordingly, the discovered sherds are *in situ* artifacts and were not disturbed by rodent burrowing, or other agents, from the present-day surface.

The mineralogical composition of the clay fraction is of ~70% IS, ~20% kaolinite, and minor amount of discrete illite, similar to that of the Sh 1-10 site. The profile is differentiated into a) the upper ~0.4 m thick part, where illite is relatively high and the saddle values are 0.73 - 0.93, and b) the lower part of the soil profile, where illite disappears and the saddle value is 0.45 - 0.57, indicating high smectitic IS composition, similar to that in the Sh 2-10 soil (Table 4b). These changes follow the increase in fine grain fractions and the decrease in organic matter at the lower part.

The Bahagi site may be interpreted as *anthropogenic* hamra, with traits of agricultural activity probably at the Roman times. Overall, this soil is less developed in comparison with

the Shamerat sequences described above (Table 2), as is evidenced by relatively low values of a* redness and relatively low magnetic susceptibility.

Figure 8. Color indices and magnetic properties of soil at Bahagi site.

North trench (NT)

The NT site (Fig. 9) is located north of Shamerat on a gentle slope occupied currently by an avocado plantation. The northward slope is facing Nahal Yasaf, which cuts the Evron ridge from east to west. The soil profile morphology indicated two pedosedimetary units, indexed below with Roman numerals.

Figure 9. Surface soil morphology and magnetic susceptibility curve at the NT site.

Unit I

Surficial disturbed horizon, 0 - 0.20/0.25 m: alternating sub-horizontal lamina of yellowish and dark brown colors with avocado leaves litter; sharp, but undulating transition.

A_p horizon, 0.20/0.25 - 0.43 m: dark reddish brown 5YR 5/6 sandy clay loam; massive; gradual transition.

BC horizon, 0.43 - 0.69 m: brown 5YR 5/8 loamy sand; finely mottled due to bioturbation by insects and worms; speckled by yellowish stains, massive; gradual transition. Although the downward transition is gradual, it is likely that the lower part of the profile is not related to the upper hamra.

Unit II

AB horizon, 0.69 - 0.95 m: 5YR 5/6 reddish brown sandy loam; angular-prismatic structure and no slickensides; black (manganese?) speckling; coarser sand grains; gradual transition.

B1 horizon, 0.95 - 1.20 m: 10YR 4/4 dark brown, loamy sand; blurred mottles of dark brown and reddish brown color; less developed angular-prismatic structure; gradual transition.

B2 horizon, 1.20 - 1.55 m (base of the trench): very dark brown 7.5YR 4/6 loamy sand; strongly prismatic; reddish spots of 0.5 - 2 cm, probably due to bioturbation by small insects. Unfortunately, the deeper layers of the sequence could not be reached. However, on the basis of earlier observations it is believed that the B2 horizon rests upon a nazaz soil. The latter is known to occur here between 1 and 2 m depth (M. Ettinger, orchards coordinator, Shamerat, personal communication).

The $CaCO_3$ content varies within the sequence, reaching maxima in the uppermost IA horizon (1.2%) and in the lowermost IIB2 horizon (1.6%), while middle horizons are practically leached (Table 3).

The grain size distribution agrees with the field observations: the BC horizon of unit I has the lowest fine fractions content, 16%, versus 30% and 27% of the upper horizon of unit I and the lower horizon of unit II, respectively (Table 3). However, the lowest horizon B2 has just 24% fine fractions content.

The magnetic susceptibility values follow the field observations and the grain size distribution. It significantly decreases in the sandier BC horizon of unit I ($\sim 18 \times 10^{-8} m^3 kg^{-1}$) versus $\sim 30 \times 10^{-8} m^3 kg^{-1}$ at the horizons below and above (Fig. 9).

In contrast to the match between those analytical parameters and the field observations, the mineralogical composition of the clay fraction here does not show clear relation to color and grain size. It is in the range of values as in other soil sections: ~75-80% IS, ~15- 20% kaolinite and saddle values between 0.66 and 0.89. In sum, this profile may be interpreted as a bi-sequential soil composed of two welded hamra soils, with a phase of sand accretion occurring between two main soil-formation episodes.

South trench (ST)

This site is located at the top of the kurkar ridge at the highest elevation in Shamerat. It is located ~200 m south of the NT site but exhibits just a single soil profile.

A horizon, disturbed, 0-0.10 m: light brown loose sand.

$AB_{p(k)}$ horizon, 0.10 - 0.40 m: reddish brown 5YR 5/6, clayey sandy loam; lighter color elongated speckles; sub-horizontal disturbed planes; a few calcitic nodules of 1 to 5 cm, calcic rhizocretions.

$BC1_{(k)}$ horizon, 0.20 - 0.60 m: lighter reddish brown 5YR 6/8 sandy loam; speckles of lighter color; a few calcitic nodules; gradual transition.

$BC2_{(k)}$ horizon, 0.60 - 0.80 m: light ochre sand 5YR 5/8; a few calcitic nodules; gradual transition.

C horizon, 0.80 - 1.25 m: yellowish 7.5YR 6/8 sand; a few calcitic nodules.

The $CaCO_3$ content (1.3-1.5%) all along the profile is higher than in other Shamerat sites. This might be derived from disintegration of the softer nodules.

The grain size distribution shows an increase of the sand fraction from 82% at the upper part to 92% at the bottom, and a parallel decrease of the fine fractions, in accord with the field description.

The mineralogical composition of the clay fraction is in the range of values as in other sites: ~70-80% IS and ~15- 20% kaolinite. The saddle values are around 0.76 in the upper horizon but 0.60 in the sandy C horizon.

5.3 Soils in additional sites

Entrance junction, Shamerat

A road cut exposes a hamra profile of about 2.5 m thickness. The natural hamra is covered by 0.30 m thick man-made materials laid upon the soil surface during construction works or road paving. The Bk horizon with densely packed calcitic nodules is located at 1.75 m below the surface of the natural soil. Only the layer above the Bk horizon was studied. This is a 5YR 5/8 reddish sandy loam and was sampled twice for regular analysis and for OSL dating (SA 600 and SA 627, respectively).

The grain size distribution of sample SA 600 is 87% sand and 13% fine fractions, exactly as at the lower parts of the ST site. The clay composition of the sample is similar to many other samples in the Shamerat sites. The $CaCO_3$ content is also as in the ST site (Table 2). The OSL age of sample SA 627 was determined to be 6.1±1.8 ky, similar to that of the upper active hamra of the ET site.

North Akko

An artificial cut exposed a ~1.8 m section (no longer existing) within a housing quarter of Akko.

0-0.27 m: an artificial layer of brownish sand mixed with road gravel stones and other modern artifacts; fine-grained mass possibly derived from the original A horizon; sharp contact.

AB horizon, 0.27 - 0.46 m: 10YR 5/4 light brown sand; structure is not well defined, but material holds together in contrast to loose sand below; effervesce, tiny calcareous nodules, sharp contact.

B horizon, 0.46 - 0.73 m: 7.5YR 5/8 reddish brown sand; effervesce; calcareous nodules, gradual transition.

BC horizon, 0.73 - 1.26 m: 2.5Y 8/4 light brown loose sand with irregular reddish mottles, related to bioturbation and filled with the B horizon material, gradual transition.

C horizon, 1.26 - 1.8 m: 2.5Y 8/3 yellowish loose calcareous sand; calcite-cemented sand patches, probably relics of original kurkar.

The 22 to 23% $CaCO_3$ content of these layers (analyzed twice) is exceptionally high. The grain size distribution of the three upper horizons shows a high sand fraction content that increases downward from 87 to 99%. Though the IS and kaolinite amounts are quite similar to those of the other sites, the saddle values of the three layers are the highest recorded in this study (Table 4). This feature might indicate an early stage in clay assemblage change towards typical hamra soils with saddle value of generally >1.

The underlying kurkar rock of the Evron ridge is exposed a few hundred meters to the south-west of this section, covered with a thin layer of loose sand with some ancient chert artifacts.

The field and analytical data suggest that this sequence is relatively young and the hamra is possibly in an incipient stage of development.

North Lohamei HaGeta'ot (NLH)

Two water pipe trenches on top of the Evron ridge, north of Lohamei HaGeta'ot, exposed two pedostratigraphic layers with an undulating unconformity between them. The field observations of the trenches suggest that the deposition of the upper layer material was accompanied by leveling off the topography that existed during the soil formation of the lower layer. Hence, local mixing of different materials may have taken place.

The two layers observed here have appearance similar to the middle and low layers of the ET site, namely, gray sandy vertic paleosol and underlying calcitic reddish paleosol. One section, of 1.8 m depth, was sampled and studied.

The upper layer is ~0.9 m thick brownish gray sand, ploughed at the top. A well-developed prismatic structure with slickensides occurs below the ploughed horizon. This soil layer contains small black organic particles and millimeter size calcitic nodules, whereas semi-spherical calcitic nodules of 2-3 cm size appear below ~0.25 m. Transition to the lower

layer is gradual. A sample taken from 0.70-0.80 m depth was dated by OSL to 102±20 ka (Table 5).

The lower layer is composed of red stiff clayey sand with abundant calcareous nodules and it resembles hamra. The nodules are hard, centimeter size, irregular, sometimes elongated in vertical dimension. This layer is less calcareous than the apparently correlative lower layer of the ET site, probably due to its higher geomorphological position. The base of the layer was not reached.

The $CaCO_3$ content is below the detection limit in both layers, despite the relatively high content of nodules in both layers.

The grain size distribution of the two vertic sandy soil samples and the top of the underlying hamra is similar, with ~57% sand fraction, whereas the lower part of the hamra is much sandier (70%).

The IS and kaolinite contents of both layers are quite similar to those of the other sites, but the saddle values are variable; the value of 0.45, the lowest recorded in this study, occurred in the vertic layer as in the vertic paleosol of the ET site (Table 4).

5.4 Soil micromorpology analysis

A detailed description of the most prominent micromorphological features of three selected sites is presented below. The summary of the micromorphological results is given in Table 3.

The Sh-1-10 site

The surface soil is developed on well-sorted sands in the range of 125-250 μm, as is clearly identifiable in thin sections. Interestingly, this is the most frequent grain size group in coastal sands elsewhere (Ronen et al., 2005; Zviely et al., 2007). The upper $A_{p(k)}$ and AB_k horizons show subangular to subrounded sand-size quartz grains, averaged 0.1 mm in size, moderately to well sorted, albeit the coarse-fine (c/f) related distribution patterns vary within the thin section. For example, the sample taken at 0.4 m depth depicts juxtaposition of chitonic, gefuric and porphyric c/f distribution (Fig. 10). Porosity is very well developed, expressed by interconnected channels related to biological activity of microfauna and root system, as well as by vughs and packing voids. Larger channels contain partly decomposed plant tissues (Fig. 10, right side), which indicate currently active soil-forming processes and the impact of vegetation as the site that is occupied by a pasture with perennial grasses.

Figure 10 also demonstrates a calcite nodule ~ 0.8 mm in size found in the AB_k horizon. The nodule, which is embedded in calcite-free groundmass, does not contain any admixtures

of clays or quartz grains, an indication of in situ formation (Wieder and Yaalon, 1974). It is composed of sparitic calcite, with signs of alteration, and probably formed on a bio-precursor (land snail shell?). Occasionally, micritic coatings occur in pores, with signs of recrystallization into microsparite. The micromorphology confirms the field identification of the upper genetic horizons ($A_{p(k)}$ and AB_k) as containing carbonate neoformation. The enrichment of a soil with secondary carbonates will be addressed further.

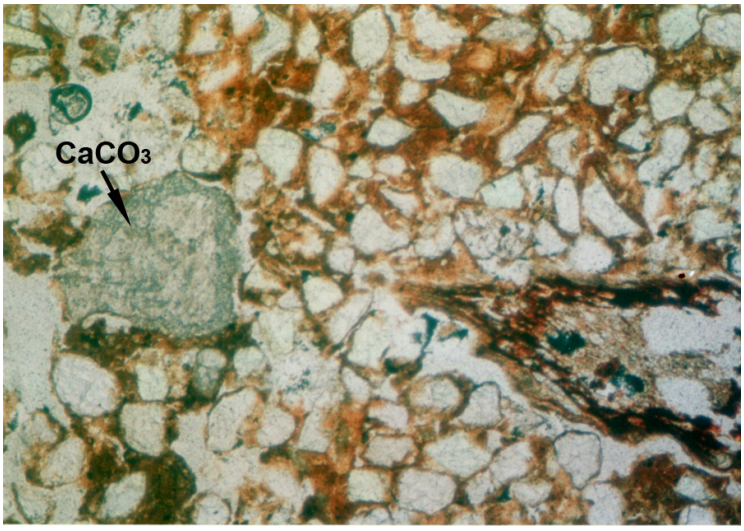

Figure 10. Microphotograph of heterogeneous, porous sandy groundmass in the A(k) horizon at the Sh 1-10 site. Note a subrounded ~ 1 mm in diameter sparitic nodule (arrow) and a strongly decomposed plant root in a larger channel (right), magnification 4x10, plane polarized light (PPL).

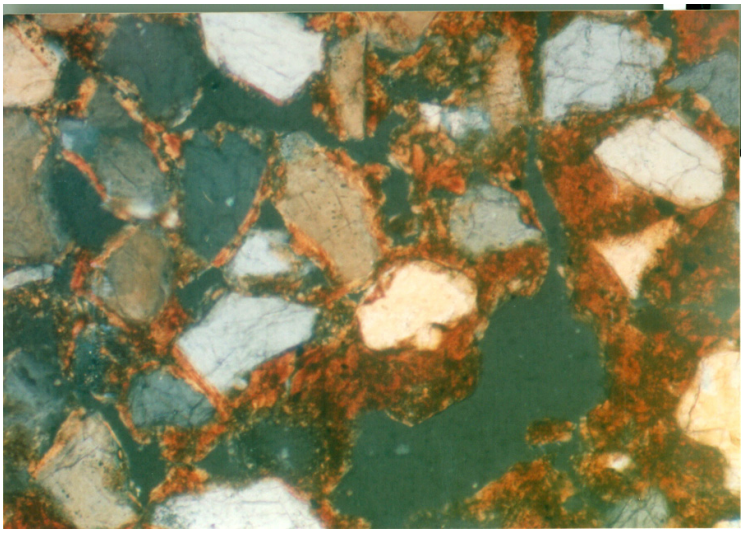

Figure 11. Microphotograph of birefringent speckled-striated aged coatings in the ABk horizon at 1-10 site (0.6 m depth); magnification 10x10, crossed polarized light (XPL).

Significantly, even the uppermost horizons show heterogeneity in the matrix, with juxtaposed reddish and brown patches in thin sections as demonstrated in Figure 10. At 0.6 m depth, in the AB_k horizon, this color heterogeneity is pronounced more intensely, and under higher magnification, abundant aged clay coatings are observed (Fig. 11). A vugh which is lined by dark reddish-brown anisotropic clay (with low optical anisotropy) is observed in Figure 10. This may result from aging and partial destruction of genuine red coating, as was demonstrated in Red Mediterranean soils elsewhere (Fedoroff, 1997) and in red paleosol in the Carmel coast as well (Tsatskin et al., 2009). Thus, although no genuine infillings in pores are found, there are micromorphological indications that clay translocation did take place during soil formation. In the course of pedogenic activity, those infillings and pore coatings were probably partially destroyed and incorporated in the matrix, creating speckled b-fabric of the groundmass (Fig. 11). A significant portion of the sand grains has 0.08 mm thick continuous aged clay coatings, along with grains either free of any coatings or covered with thin and discontinuous ones.

Large septaric nodules were examined in thin sections as well. One such nodule (from 0.4 m depth, Fig. 4) has a very complex microfabric (Fig. 12). The nodule's outer zone is composed of brown stained clay, strongly impregnated with microsparitic, in which ~40% of quartz sand grains are incorporated (Fig. 12, right corner). This calcite-clay zone merges with a nearly pure calcite zone, showing several zones of recrystallization around pellets (Fig. 12, center). Quartz grains are distributed randomly. At the left corner of Figure 12 one can see quartz-containing non-stained calcite, which probably formed at an earlier stage as a discrete nodule but was later incorporated into a larger nodule. Eventually, a complex nodule formed around numerous pellets as centers of crystallization. At a later stage it was fractured and secondary sparitic calcite crystals grew along the fractures.

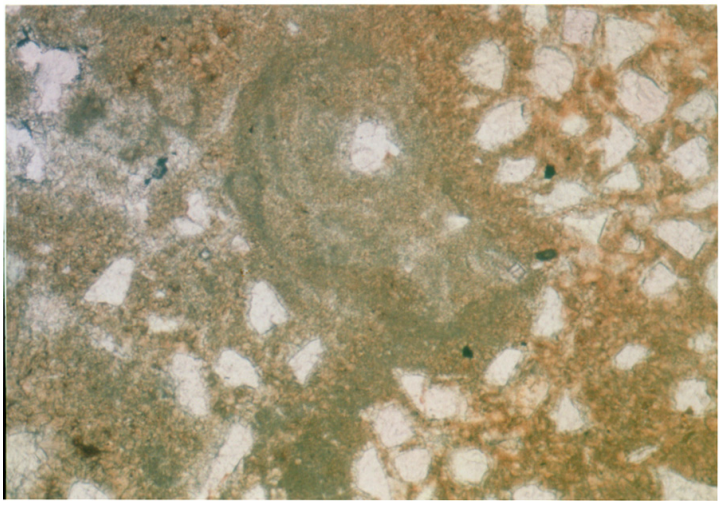

Figure 12. Microphotograph of a septaric nodule shown on Figure 4. Note strongly heterogeneous fabric showing at least three zones: left - non-stained calcite containing quartz sand , center - pure calcite showing several zones of recrystallization around pellets, right - strongly impregnated with microsparitic brown stained clay; the internal structure testifies to a number of stages of recurrent growth and disintegration (Wieder and Yaalon, 1982); magnification 4x10, PPL.

Taking into account earlier concepts of $CaCO_3$ formation in Israeli soils (Wieder and Yaalon, 1974, 1982), we propose that such complex microfabrics indicate a long history of in situ carbonate formation, of recurrent growth and disintegration stages. In addition, abundant opaque Fe-Mn stains occur.

Aged clay coatings fabric is also found in the Sh 2-10 site in deeper horizons, whilst the uppermost horizon shows strong humification, manifested by the groundmass color, complex porosity pattern, charcoal and fresh tissues in channels. These features allow us to suggest that rubification as identified in the 1-1 site, was rather obscure by humification under better watering conditions at the Sh 2-10 site.

Table 3. Micromorphological description of samples from selected sites

Sites	Structural features	c/$f_{40\mu m}$ ratio	Fine mass	Calcareous features	Other Pedofeatures	Identification
Sh 1-10 $A_{p\,(k)}$ horizon	Compacted with abundant bio-channels, vughs and vesicles	8:2	Heterogeneous including dark brown isotropic and reddish-brown, speckled-striated	Rare nodules of biologigic origin and pore infillings, along with strong large differentiated nodules	Common aged clay coatings around matrix grains; strong brown clay coatings along the planes; decomposed plant tissues	Strongly developed calcareous polygenetic hamra-husmas
AB_k horizon	Compacted with abundant bio-channels, vughs and vesicles	8:2 to 9:1	Brown Striated-strial		Aged clay coatings , no plant residues	
BC_k horizon	Compacted	9:1	Heterogeneous	Only rare nodules		
NT Unit I, A_p horizon	Dense, with minimal porosity but heterogeneous due to juxtaposition of looser and denser zones	9:1	Brown speckled-striated uneven	None	Matt brown strongly aged coatings on some grains, as well as zones of striated b-fabric in matrix; some black-brown opaque stains and disintegrated charcoal	Moderately developed quartzic hamra
BC horizon	Crumbly, with 20% porosity presented by channels and vughs	9:1	Reddish-brown Uneven speckled	Absent	Aged coatings on some grains and as elongated zones, occasionally strongly oriented clay coatings; speckles of reddish Fe amorphous impregnations	
Unit II, AB horizon	Crumbly, with 30% porosity presented by biochannels and vughs; strong weathering of plagoclase	9:1	Reddish-brown Uneven speckled-striated	Sparitic calcite linings on walls of some biochannels	All grains with aged coatings, zones of higher clay content with speckled-striated b-fabric unevenly distributed, probably due to bio-turbations; reddish and yellowish zones of aged coatings.	More strongly developed hamra
B1 horizon	Less crumbly, denser, similar	8:2	Reddish=brown Uneven speckled-striated with yellowish striated zones	Very rare degenarted micritic coatings	Strongly developed b-fabric of aged coatings coalescing with matrix; however, occasionally coatings are better delineated either as in pores or around grains	
B2 horizon	Porosity strongly decreases, but biochannels present	9:1	Reddish=brown Uneven speckled	Very rare micritic nodules	Poorly developed aged coatings; developed opaque ~ 1mm in diameter Mn nodules with concentric outer rim and b-fabric	Hydromorphic hamra?
ET Layer 1	Dense heterogeneous, zones of compacted grains juxtaposed with better aerated zones due to biochannels	8:2	Dark brown, speckled heterogenous	None	Brown zones of aged clay coatings with zones devoid of b-fabric; ferruginized remnants of plant tissues in root channels (modern), opaque Fe-Mn dense nodules with diffuse boundary or tiny speckles scattered all	Moderately developed humic semi-hydromorphic hamra
Layer 2	Very dense with sinuous planes, few vughs	9:1	Undifferentiated with striated to strial zones along planes	None	Few aged clay coatings; tiny black opaque Fe/Mn nodules along with brown opaque Fe differentiated nodules 0.2-0.5 mm and coatings	grumusol (vertisol)
Layer 3	Melange of two types of materials: strong red clay incorporating abundant quartz grains (less than 30% of the slide); major phase is strongly calcareous mass, both aggregated and welded, with planes completely filled with sparitic infillings as well as distinct well-lineated clay coatings	Clay mass: 9:1 Some zones of calcareous mass: from:4:6	-	-	-	Melange of Strongly developed hamra and brecciated polyphase calcrete, possibly incorporating kurkar derivatives

The NT site

The uppermost A_p horizon shows in thin sections a well sorted sand-size quartz skeleton grains embedded in a dense, non-aggregated brown fine-grained mass (Fig. 13). However, the sample contains occasional oval gefuric aggregates, embedded in porphyric mass. These aggregates may be ascribed to bioactivity within the upper soil, despite compactness and disaggregation, which are likely caused by modern irrigation. The almost isotropic nature of the groundmass seems to be related to humus enrichment, although under higher magnification speckled b-fabric is recognizable, as well as strongly aged thin clay coating around quartz grains. The thin section shows rare irregular opaque and partially disintegrating vegetal charcoal and charred particles which testify for humification process.

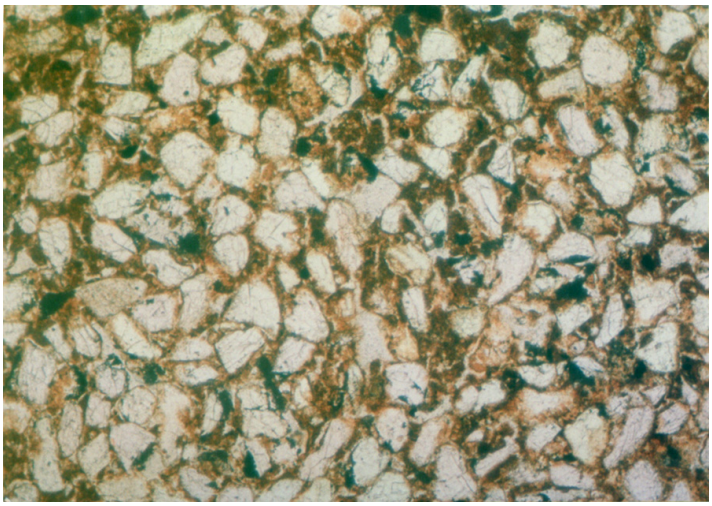

Figure 13. Microphotograph of dense, non-aggregated sand-sized rich microfabric in the A horizon at NT hamra; magnification 4x10, PPL.

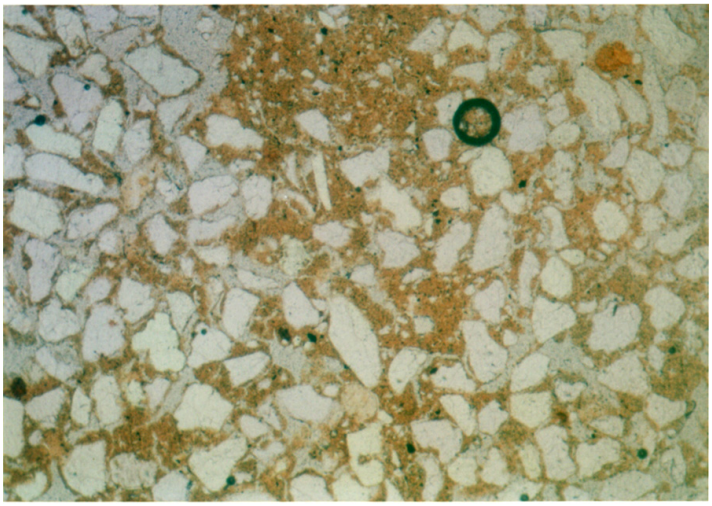

Figure 14. Microphotograph of two differing zones in the AB horizon at NT hamra: silty clay-rich (center) embedded in a sand-rich mass; magnification 4x10, PPL.

The $AB_{(k)}$ horizon at ~ 0.6 m depth shows considerable heterogeneity in the matrix, with juxtaposed reddish-brown silty clay patches and nearly colorless coarse-grained patches (Fig. 14). Under crossed polarized light silty clay zones show a striated b-fabric and may be interpreted as strongly aged clay coating that initially originated in, and around, larger pores that eventually collapsed at a later stage of pedogenesis, and not around grains. Occurrence of rare sparitic coatings in channels lead to codify the horizon with (k) subscript.

At 0.9 m depth, in the same horizon, the amount of fragments of calcite coatings, disintegrated in a later stage of pedogenesis, increases and the porosity is higher. Black manganese opaque nodules indicate the former prevalence of hydromorphic conditions (see Tsatskin et al., 2008).

In the B1 horizon the heterogeneity is much more pronounced and pore space reaches ~20%. Pores are largely represented by bio-related channels. The groundmass is composed of more isotropic and less isotropic patches. The latter show speckled b-babric with some striation. Zones of genuine striated b-fabric are rare.

In sum, no strong calcite deposition is found in thin sections, albeit with expressed variability along the profile. These variations suggest that this is a polygenetic, bi-sequential soil in which an upper hamra (unit I) is micromorphologically distinct from the hamra in the lower part of the profile (unit II) in terms of stronger humification and absence of carbonate accumulation.

The ET site

The upper layer appears in thin sections as dark brown, heterogeneous dense mass in which strongly compacted zones are juxtaposed with better aerated zones showing biochannels and vughs. The channels contain occasionally ferruginized remnants of plant tissues. Brown zones of speckled-striated b-fabric due to incorporation of aged clay coatings into the groundmass are juxtaposed with zones devoid of b-fabric. Opaque Fe-Mn dense nodules with diffuse boundary, or tiny opaque Fe-Mn speckles, are scattered all over. These features allow us to classify the layer as moderately developed humic hamra.

The middle layer appears in thin sections as a dark, very dense mass with ~60 % well sorted sand. Sinuous planar voids (fractures) are characteristic features of the layer, whilst vughs and channels are few. Under crossed polarized light the matrix shows occasional striated to strial zones, usually along planes. Aged clay coatings are almost indiscernible. Tiny black opaque Fe/Mn nodules along with brown opaque Fe differentiated nodules 0.2-0.5 mm are numerous. The micromorphological features demonstrate typical vertic properties, although the amount of sand in the soil is substantial. These diagnostic features

were earlier described in Israeli vertisols (grumusols), as well as in paleogrumusols e.g. in the Nahal Hadera outlet (Tsatskin et al., 2008) or in the upper (grumusol) member of the Netanya paleosol complex (Gvirtzman and Wieder, 2001).

The lower layer appears in thin sections as a mélange of two types of materials: 1) less than 30% of the slide is strong red clay incorporating abundant quartz grains; 2) the major material is strongly calcareous mass, both aggregated and welded. It shows planes completely filled with sparitic infillings, as well as distinct well-lineated clay coatings (Fig. 15). Aggregation of the calcareous mass into ooid-like structural units suggests that calcrete was probably brecciated prior to the phase of agglomeration, when the individual aggregates welded. In addition, sole calcrete aggregates contain ~30% of quartz, which suggests that at its earlier stage the primary material was kurkar. Hence, a former calcrete layer, which was not immediately obvious in the field, is recognized in thin sections, and may be classified as a complex polyphase calcrete, possibly incorporating kurkar derivatives.

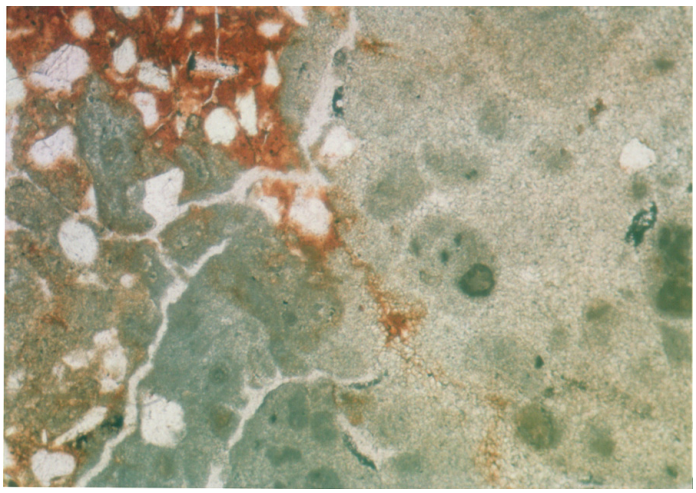

Figure 15. Microphotograph of a mélange of dense calcrete and strong red sand-rich hamra material of the lower layer at ET sequence, note several micritic crystallization centers within the microsparitic mass of calcrete; magnification 4x10, PPL.

5.5. Clay mineralogy

The dominant clay mineral in all soil samples is randomly-ordered IS with a narrow content range between 65 and ~85%, mostly between 70 and 80%. However, its composition, as indicated by the saddle values, is fairly variable; the lowest saddle value of 0.45 was recorded in the grayish vertic sandy soil detected at both the ET and NLH sites and in the B2 horizon of the Bahagi site, indicating prevalence (about 75%) of smectitic interlayaers. This value is within the range of 0.35-0.5 found in sandy vertisol samples near

Bet Dagan (Sandler et al., 2009). The highest saddle values of 0.91-0.95, indicating illitic composition, were recorded in shallow carlcareous sandy hamra at north Akko and in one sample of the Bahagi site. These values are similar to those in loess soils of the northern Negev and are somewhat lower than in typical leached hamra samples of >1 saddle values (Sandler et al., 2007; Sandler et al., 2009). Most other samples have saddle values between 0.50 and 0.80. Kaolinite is always secondary in amount, with a content range of 15 to ~ 25 %. The IS and kaolinite content variability is complementary as the other mineral amounts are rather negligible. Illite is present in very low amounts of up to 10%. The mixed-layer mineral kaolinite/smectite (KaS) was identified in about a third of the samples and was suspected in a few more. Quartz is present in trace amount in the clay fraction (<2 %) of most samples and goethite was identified in about half of the samples. Chlorite is below detection limit in most samples and was suspected to occur in trace amount in a few.

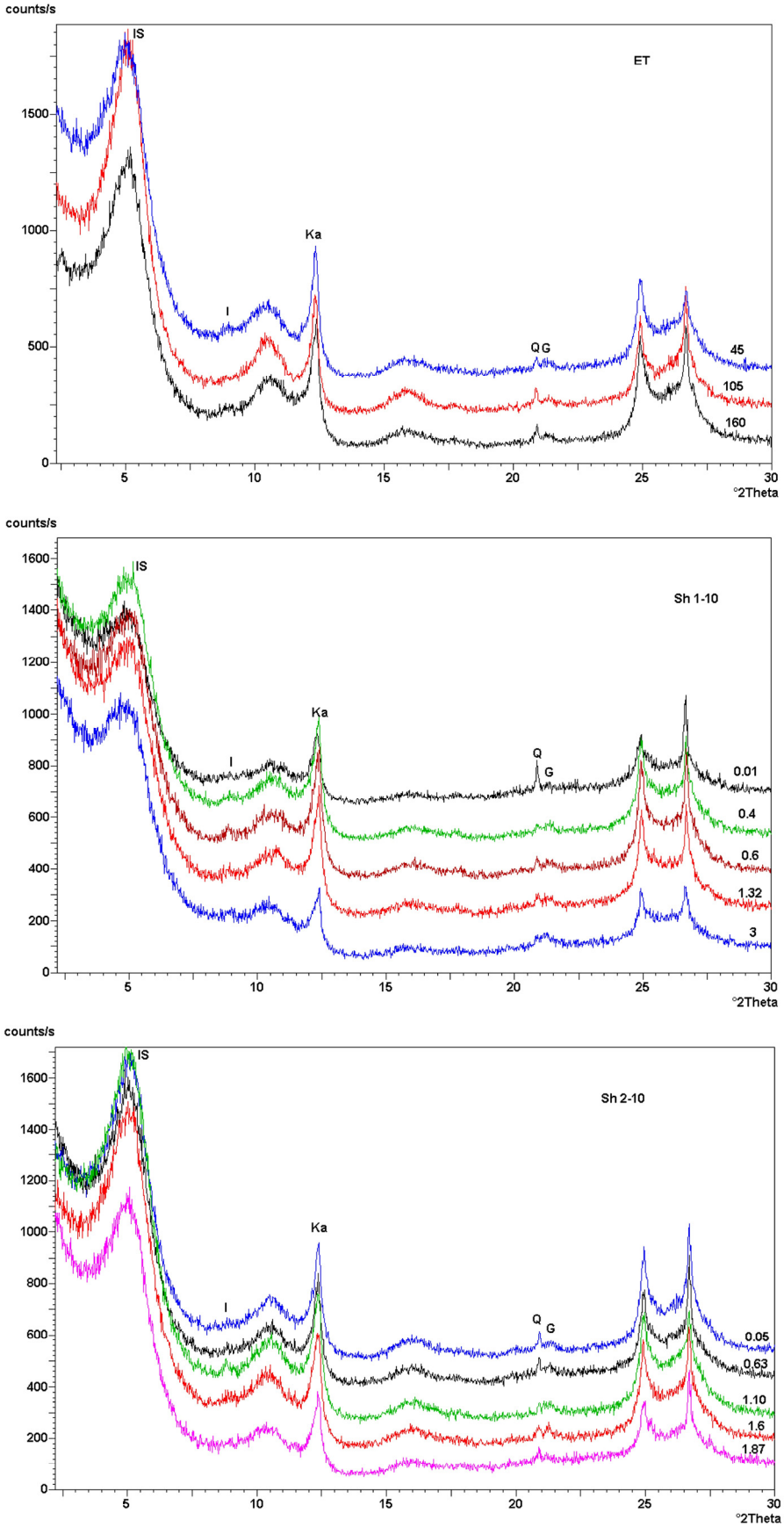

Figure 16. Diffractograms of the clay fraction (glycolated) of: a) Sh 1-10; b) Sh 2-10; c) ET.

The Sh 1-10 and Sh 2-10 sites have similar clay assemblages, but the saddle values, which are uniform along each of the profile, are significantly different. The topographically lower lying Sh 2-10 site has a saddle value range of 0.50 - 0.57, whereas the Sh 1-10 site upslope is 0.72 - 0.78.

The clay assemblage of hamra and related soils in the Akko-Shamerat area, including the strong red soil from the base of the ET and the Lohamei HaGeta'ot trench, is different from hamra soils studied thus far either in the Haifa Bay subsurface (Sandler et al., 2007) or surface hamra soils in central Israel (Sandler and Herut, 2000; Sandler et al., 2009). In those and earlier studies (Koyumdjiski et al., 1988), the clay assemblages of leached mature hamra showed kaolinite amount of up to ~ 50% and even higher, whereas the IS amount was less than 60% with high saddle values of > 0.90. The illite amount range was generally 10-30%, significantly higher than that in the hamra soils studied here.

Table 4. Mineralogical composition of the clay fraction, semi-quantitative (%)
a. soils on the eastern ridge slope

location	depth, m	IS	saddle	kaolinite	illite	quartz	goethite	KaS
Sh-1-10								
4	0.01	75 - 80	0.72	15	<5	<2	+	+
11	0.40	70	0.73	20 - 25	5	<1	+	+
18	0.60	65 - 70	0.73	20 - 25	5	<1	+	+
22	0.95	75	0.77	20	5	<1	+	+
26	1.32	75	0.76	20	<5	<1	+	+
31	1.9	75	0.73	15	5	<1	+	+
34	3.0	80	0.78	10 - 15	<5	<1	-	?
Sh-2-10								
0	0.05	80	0.50	15 - 20	?	<1	+	?
2	0.25	80	0.51	15	<3	<1	+	+
4	0.63	80	0.57	15	?	<1	+	-
5	0.75	75 - 80	0.51	20	<3	<1	+	?
7	1.10	75 - 80	0.53	15 - 20	<3	<1	+	?
9	1.6	75 - 80	0.55	15 - 20	<5	<1	+	?
11	1.87	80	0.54	15	?	<1	-	-
12	2.1	80 - 85	0.69	15	<3	<2	?	?
ET								
	0.45	80	0.63	15	<5	<1	+	+
	1.05	80	0.45	15	?	<1	?	?
	1.60	75	0.48	20	<3	<2	+	?

b. soils on the western ridge slope and additional sites

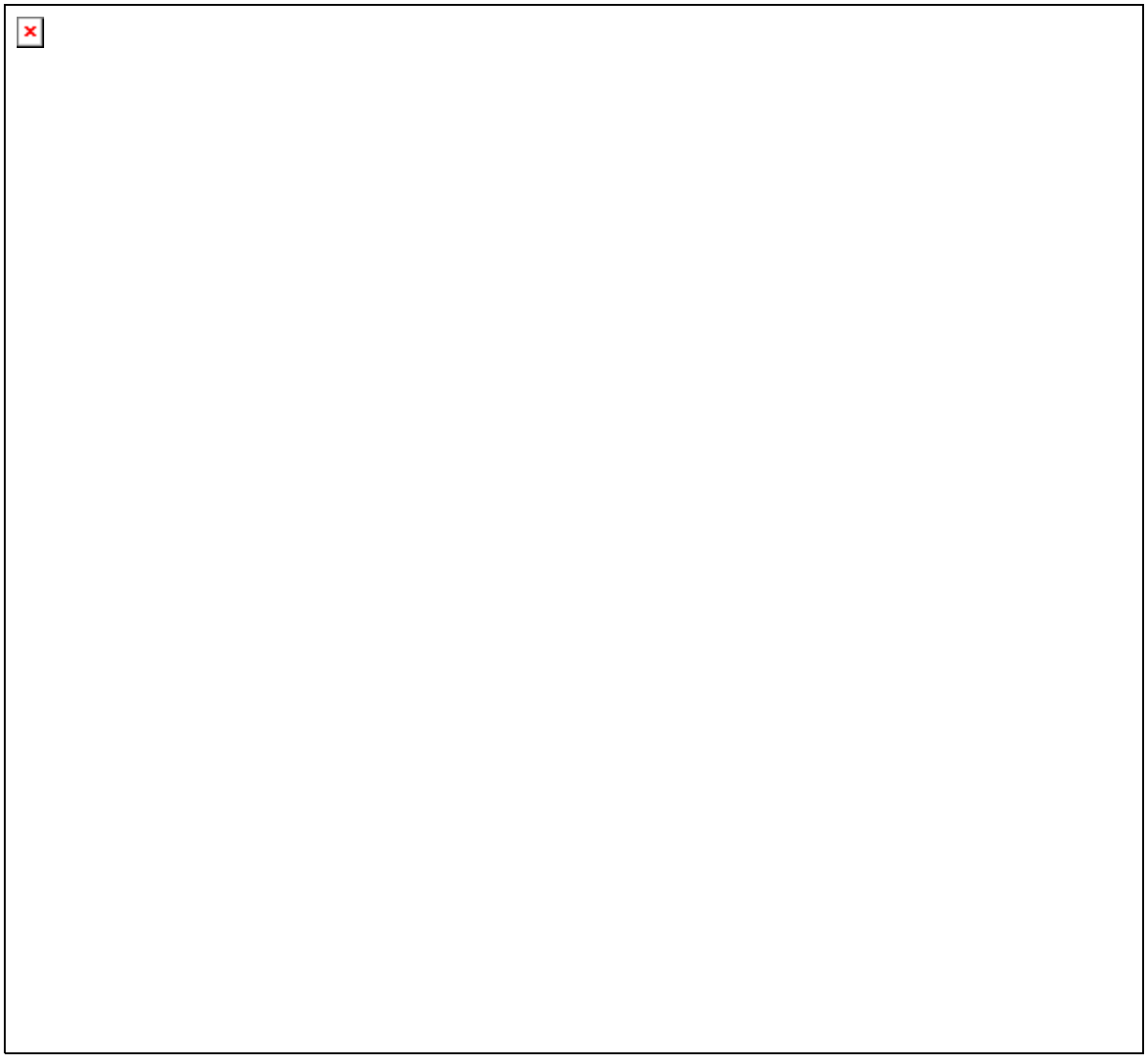

5.6 The OSL and ^{14}C ages

The OSL burial ages obtained for the base of the hamra and the underlying loose sand at depths between 0.6 and 2.6 m at the Sh 1-10 and Sh 2-10 sites are all older than ~250 ky. Previous OSL and ESR dating of the Evron ridge indicated ages older than 300 ka for the upper kurkar samples at the Evron quarry (Porat and Ronen, 2002). An additional result of this project is the establishment of "young" OSL dates in some sections. The interpretation of such large chronological window is not simple. We tentatively propose that the last major windblown episode of coastal sand accumulation from the shore took place ~250 ka ago. Between this Middle Pleistocene sand accumulation event and the Last Glacial event the southern Evron kurkar ridge apparently did not undergo any pronounced soil-geomorphic changes, because parent sands for major soils have not been exposed to sunlight for at least 250 ky. In any event, based on the OSL dates, the sand in the Shamerat area cannot be

considered recent as previously assumed (e.g. Sivan, 1996). However, windblown contribution from the Haifa Bay beach is plausible for the uppermost part of the studied sequences.

Alternatively, in other locations the active hamra soil is formed on parent sands of much younger age. The base of the upper layer hamra at the ET site at the toe slope of the ridge yielded the age of 6.1 ±1.9 ky. Although the OSL data is rather scattered, the average age provides a reasonable estimation of the timing of sand accumulation given that cultivation was absent or minor. The same layer, a few hundreds meters to the west (the entrance to Shamerat), though much thicker, yielded a similar 6.1 ±1.8 ka age at the 1.7 m depth, just above a calcic horizon. This artificially-cut section at the ridge top seems to exhibit a single profile. A few hundred meters to the south, a historical anthropogenic hamra profile yielded younger, but similar, OSL and ^{14}C ages. A sample at 0.8 m yielded an OSL age of 3.0±0.5 ka whereas the ^{14}C uncalibrated ages of the underlying and overlying samples were 3.6 and 2.5 ky, respectively. These dates are consistent with the Roman ceramic artifacts being *in situ*, i.e. of a ~2,000 years surface, and were not transported by biological reworking. It is therefore concluded that the uppermost and currently active hamra soil in certain places is being formed on sands buried some 6 to 3 ka ago.

At the ET site, the underlying grayish vertic paleosol yielded OSL age of 15±4 ky. A few kilometers to the north this apparently same paleosol is exposed at the highest part of the Evron ridge (NLH site) but yielded a significantly older age of 102 ±20 ky. It seems, therefore, that during the last glacial period the region experienced sand accumulated at the eastern part of the ridge, followed by flooding and hydromorphic conditions. The vertic paleosol overlies a calcic horizon of older red hamra that its parent material was buried around 200 ka ago (4 ages, Table 5). Accordingly, the hamra could have been developed between ~200 to ~100 ky.

Table 5. Dating
a. OSL results

Sample	Location/material	Depth (m)	K (%)	U (ppm)	Th (ppm)	Alpha (μGy/a)	Beta (μGy/a)	Gamma (μGy/a)	Cosm. (μGy/a)	Total dose (μGy/a)	De (Gy)	O-D (%)	No. of discs	Age (ka)
SA-604	Sh 1-10, sand	1.5	0.61	0.3	1.2	1	440	219	182	842±28	233±76	27	5/6	>276±90
SA-606	Sh 1-10, mottled soil	0.6	0.63	0.6	2.7	3	518	314	203	1037±30	265±80	12	5/5	>256±72
SA-607	Sh 2-10, sand w/lamina	2.1	0.62	0.4	1.3	1	458	231	162	853±28	214±32	11	7/7	>251±38
SA-608	Sh 2-10, sand	1.3	0.58	0.5	2.3	2	467	276	178	923±29	286±86	26	7/7	>310±93
SA-623	ET, layer 3, red soil w/calcrete	1.95	0.56	0.8	4.6	4	539	400	165	1107±31	238±64	24	13/13	215±58
TT-OSL											205±20	8	8/8	185±19
SA-624	ET, layer 3, red soil w/calcrete	1.6	0.37	0.7	3.6	3	388	306	172	868±28	183±57	28	15/15	211±66
TT-OSL											169±38	19	8/8	195±45
SA-625	ET, layer 2, sandy vertic soil	1.3	0.56	0.9	5.0	4	559	427	178	1169±35	17.4±4.7	25	17/17	15±4
SA-626	ET, layer 1, upper hamra	0.5	0.22	0.7	3.3	3	288	260	210	762±29	4.7±1.4	30	13/17	6.1±1.9
SA-627	Entrance, base of upper hamra	1.75	0.59	0.5	2.1	2	468	269	162	908±32	5.6±1.6	58	13/17	6.1±1.8
SA-632 (SA-634)	Bahagi, hamra, B_2 horizon	0.8	0.5	0.6	2.8	3	446	290	229	968±33	2.9±0.5	17	16/16	3.0±0.5
SA-639	NLH, sandy vertic soil	0.75	0.45	0.8	3.6	4	455	333	193	986±33	101±19	30	15/19	102±20

Comments: Only a small number of measurements was carried out on most of the old samples, due to the very long time needed for such measurements.
The ages for samples 604-608 are minimum ages, and they could be much older. The old ages for samples 623 and 624 are supported by similar TT-OSL ages.
There is a very large scatter in the young vertisol and hamra samples, due to bioturbation and mixing.
O-D is over-dispersion, an indication of the scatter within the sample related to sample inhomogeneity. No. of discs
is the number of measurements used for age calculations out of all measurements

b. AMS ^{14}C results at Bahagi site

Sample	Poznan no	Age	Comments
Ap, 0.45 m depth	Poz-37936	440 ± 30 BP	Melanized topsoil
B1, 0.73 m depth	Poz-37938	2030 ± 40 BP	Ceramic sherds
BC, 1.20 m depth	Poz-37939	3590 ± 70 BP	Subsoil

5.7. Grain size

The clay fraction content in the studied soils ranges between less than 1 to 36% and the silt fraction from less than 1 to 13% (Table 3). There is a general positive correlation between the silt and clay fraction, as expected, but it seems to consist of two different lines that might reflect different processes (Fig. 17). The general trend within a profile is of decreasing content of fine fractions from the upper part down to the sandy parent material. This trend is accounted for, at least partly, to continuous accumulation of airborne fine material within developing soil profiles (Yaalon and Dan, 1967; see review by Dan et al., 2007). Accordingly, grain size distribution may reflect the relative ages of soils, i.e. the duration of soil formation. For example, the lowest content of silt and clay fractions was found in the North Akko site (9% and 4%, respectively). The exceptionally high $CaCO_3$ content and other features there suggest that this profile is relatively young. The highest content of the fine fractions, on the other hand, was recorded in old soils and plaeosols at the ET and NLH sites, where clay is about 36% and silt about 13%. It seems that the high clay content of the active hamra, the upper layer of the ET site, is inherited, at least in part, from the lower vertic soil. This is supported by the relatively high Fe and Mn oxide particles, which is also exceptional for recent surface hamra. A few profiles show increase of the fine fractions content below the topsoil, due to downward migration and clay accumulation in the AB or B horizons.

The geomorphological position controls the distribution of fine material along landforms via slope wash and deposition of on lower slopes. Thus, the upper slope Sh 1-10 site has 18% whereas the lowe Sh 2-10 site has maximum clay content of 32%. Similarly, the top ST site has maximum clay content of 16% versus 23% of the nearby NT profile on a northward slope (Table 2). In sum, grain size distribution in hamra soils is controlled by several

processes and additional research is needed to decipher which process control the different clay versus silt ratios.

5.8. $CaCO_3$, SOC and ^{14}C concentration

The samples studied can be divided into three distinct categories with respect to their $CaCO_3$ concentration: 1) below the detection limit, i.e. 0.8%. Most samples are included in this category, e.g. in Sh 1-10, Bahagi, and NLH sections, despite the variable content and distribution of carbonate nodules; 2) the $CaCO_3$ concentration is in the range of 1-6%. This category includes the Sh 2-10 site, the Shamerat entrance soil and the nearby ST section, whereas in the NT section such samples alternate with samples associated with the first category; 3) $CaCO_3$ concentration is >10%. This category includes the lowest layer of the ET site, on one hand, and the apparently youngest profile of North Akko, on the other hand.

About half of the samples have SOC concentration below the detection limit, 0.1%. However in some soils the SOC varies between 0.11 to 0.43%. The highest value is recorded in topsoils, especially in the upper horizons of the vertic soil/paleosol (NLH and ET sites). The low SOC concentrations in the studied hamra are in a good agreement with earlier observations on coastal hamra soils (Koumdjiski et al, 1988), in which low SOC values correlate with low clay amounts.

Despite such low SOC concentrations, it was possible to detect by AMS the ^{14} C concentration in the Bahagi site. Recall that the topsoil there is a dark-colored sandy loam and has the highest SOC (0.17%) in the profile, which is indicative of melanization process. The subsoil, with 0.11% SOC and rare archaeological ceramic finds, has a typical hamra red-brown coloration. Radiocarbon ages increase with depth from 0.44 ky at 0.45 m depth to 2.03 ky at 0.73 m depth and to 3.59 ky at 1.10 m depth (Table 5b). Previous radiocarbon analysis in the Akko area was performed on clayey vertisols (Becker-Heidmann et al., 2002), in which an age increased from ~1,000 y in topsoil to ~5,000 y at 1.8 m depth. These ages were interpreted as the rate of organic carbon rejuvenation, i.e. the rate of pedoturbatuions, and not as reflecting a real chronological sequence. In loamy hamra soils, organic carbon is assumed to be largely associated with finely dispersed Fe oxides and oxyhydroxides along with clays (Singer, 2007), and hence the ^{14} C concentration may reflect, as elsewhere, the rate of carbon dynamics and stabilization (Cherkinsky and Brovkin, 1993; Brunner, 2010). However, in the Bahagi site the topsoil is distinct from the archaeologically related subsoil, which allows us to assume that the latter was once on the surface and was later covered by

moving sands that underwent pedogenic reworking. If so, the ~2 ka ^{14}C age at 0.73 m depth may be interpreted as the age of soil burial.

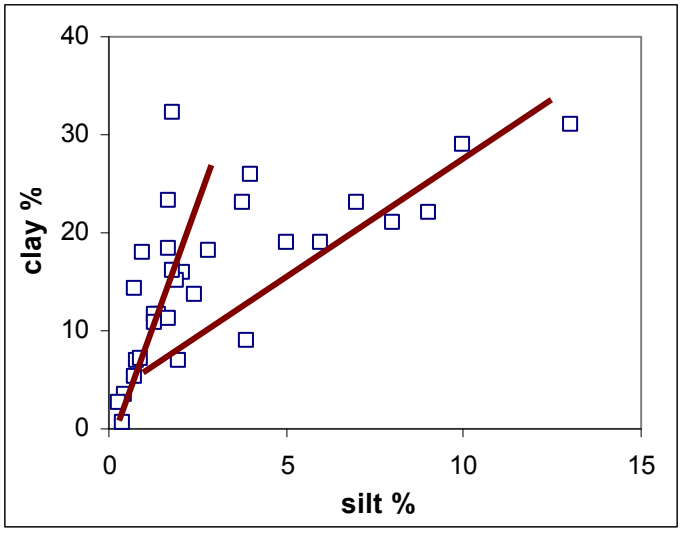

Figure 17. Clay versus silt fractions plot.

6. DISCUSSION

A variety of surface soils, some of them complex, has been detected in the investigated area, which is limited to the Akko-Lohameh HaGet'ot part of the Evron ridge. Hamra type soils are known to develop on sandy parent materials in upper topographic positions along coastal plain catena. They are characteristically red in color and are commonly considered as typical for current Mediterranean climate. In the studied area, surface and subsurface related soils show a strikingly large chronological range within a toposequence in a closely spaced landscape pattern: from Holocene to late Middle Pleistocene. The active soils of the eastern slope of the kurkar ridge at Shamerat, which have redness and magnetic properties of typical hamra soils, as known from south of the Haifa bay, were found by integrative pedologic and mineralogical studies to be polygenetic and to inherit the typical parameters from a previously developed hamra profile.

One of the key properties of hamra soils studied is the presence or absence of secondary carbonates. Leaching of carbonates in hamra soils was assessed by Dan (1983) from the viewpoint of hamra evolution over time. Dan (1983) surmised that carbonate leaching in earlier stages of hamra development was more intense than that in the later stages. Wieder and Yaalon (1974, 1982) emphasized the role of micromorphology and viewed various types of $CaCO_3$ nodules as depending on soil fabric and stages of soil development. In the studied area we distinguish between hamra soils devoid of nodules and soils containing conspicuous

septaric nodules or rhizoliths. The hamra soils on the eastern slope catena are developed on sands dated by OSL to >250 ka. These soils can be defined as both actively functioning soils with strong bioactivity, as manifested by semi-decomposed organic residues in topsoil, and as relict soils recording features from past soil-forming episodes. The clear evidence for the relict features are the large septaric nodules whose inner fabric is much more complex than any type of nodules previously found in Israeli hamra and husmas soils (calcic soils evolved out of hamra) (Wieder and Yaalon, 1974). The nodules provide evidence for carbonate leaching and clay illuviation, as well as in situ growth and transformation of micritic and sparitic crystals. These processes cannot develop simultaneously and rather represent different stages of development constrained by environmental change, e.g. groundwater table fluctuations. This new evidence is in line with recent studies that provided evidence that many surface and near-surface hamra soils are actually complex polygenetic pedogenic entities (Tsatskin et al., 2008, 2009). Accordingly, the terms "modern" or "recent" soils with regard to surface hamra soils should be used with caution.

Some additional features seem to represent environmental change as well. One of those is a very high degree of churning of the subsoil with mole burrows reaching up to 3 m depth. The other feature is the unique clay mineralogy in the Akko-Shamerat area hamra soils. The soils here differ from hamra in the central part of the Israeli coastal plain and the subsurface of the Haifa Bay by the dominance of IS of high to medium smectitic composition and the low amounts of kaolinite and illite. All these features suggest that the polygenetic soils at the Sh-1-10 and Sh-2-10 sites underwent a stage of *restricted leaching and occasional hydromorphism*, which are partially preserved in them, now as relict features. The original upper part of the old profiles has been truncated, the deeper parts were exposed, and the current profile reactivated the older one. In terms of Schaetzl and Anderson (2005) such partial soil records are called "palimpsest that has information written on it" (p.619), albeit in a restricted way. At the current state of knowledge there is no direct dating of the old profile formation, the time of truncation and the time of stabilization and soil reactivation. Indirect indication for the age of those processes might be found in the age of a nearby buried paleosol and in prehistoric findings.

Since the 1930's geologists tried to define and record prehistoric finds in the sediments of the Galilee coastal plain. For example, Avnimelech (1943) described in detail such occurrences from water drillholes. Later archaeological-geological surveys were systematically conducted by Avraham Ronen and colleagues in the 1970s (e.g. Gilead and Ronen, 1977; Ronen, 1991), who found out that Acheulian handaxes are frequent in the

surface soil of the Galilee coastal plain , especially near the Early Lower Palaeolithic site of the Evron Quarry. These archaeological findings apparently provided an important chronological constraint for the age of the uppermost sequence of the Evron ridge. Significantly, they are in good agreement with the current OSL dates, obtained via application of the most updated methodologies.

The ~200 to ~100 ka ages, which constrain the formation time of the buried calcic paleo-hamra at the ridge toe at Shamerat could have tentatively been correlated to that of the exhumed hamra/husmas with the septaric nodules. The erosion of the covering deposits may have taken place during the last glacial, the time of sand accumulation and vertic soil formation above the ancient calcic hamra.

The sandy vertic soil with well-developed calcitic nodules is locally exhumed, as observed to the north of Shamerat area where it is an active agricultural soil. However, more research is needed to properly understand the development of the exhumed vertic soil near Lohamei HaGeta'ot. At the same time its two dated samples indicate that its parent material accumulated to the east of the Evron ridge during the last glacial, and might document the gap between the formation time of the ancient top-ridge hamra and the time of its re-activation during the Holocene.

All hamra soils lacking septaric nodules show in thin sections some reddening, aged clay coatings on sand grains; occasional increase of illitic component in the mixed-layered IS mineral phase, and are likely related to a young Holocene group, as evident by numerical dating. We propose that young active hamra soils have been formed on sands of the youngest eolian sand depositional episode of the Holocene (Zvieli et al., 2007) when the source of sand was the Haifa Bay shore. In conclusion, soil toposequences in the southern part of the Evron kurkar ridge reveal a mosaic of chronologically heterogeneous soils some of which may have recorded periods of surface instability, and sand accumulation from adjacent eroded surfaces.

ACKNOWLEDGEMENTS

The work was supported by grant ES-14-2010 of the Ministry of Infrastructure. Additional support from the Research Authority of the University of Haifa (for Tsatskin) is gratefully acknowledged. R. Binstock analyzed SOC and M. Kitin analyzed $CaCO_3$. Chana Netser prepared the maps. Special thanks are due to M. Ettinger of Shamerat for his willing assistance.

REFERENCES

Becker-Heidmann, P., Andresen, O., Kalmar, D., Scharpenseel, H-W., Yaalon, D.H., 2002. Carbon dynamics in Vertisols as revealed by high-resolution sampling**.** *Radiocarbon* 44 (1), 63–73.

Brunner, I. (ed.), 2010. *Belowground Carbon Turnover in European Forests – State of the Art*. COST Action FP0803 Conference January 26–28, 2010. Swiss Federal Institute for Forest, Snow and Landscape Research WSL, Birmensdorf.

Cherkinsky, A.E., Brovkin, V.A., 1993. Dynamics of radiocarbon in soils. *Radiocarbon* 35 (3), 363-367.

Dan, J., 1983. Soil chronosequences in Israel. *Catena* 10, 287-319.

Dan, J., Fine ,P., Lavee, H., 2007. *Soils of the Land of Israel.* The "ERETZ" Series Geographic Research & Publication, 309 pp. (in Hebrew, with English summary).

Dan, J., Koyumdjiski, H. (eds), 1979. *The classification of Israel soils*. The Volcani Center, Bet Dagan (in Hebrew, with English summary)

Dan, J., Yaalon, D.H., Koyumdjisky, H., 1969. Catenary soil relationships in Israel, the Netanya Catena on coastal dunes of the Sharon. *Geoderma* 2, 95-120.

Evans, M.E., Heller, F., 2003. *Environmental Magnetism. Principles and Applications of Enviromagnetics*. Academic Press, San Diego, London, Burlington.

Emery, K.O., Neev, D., 1960. Mediterranean beaches of Israel. *Israel Geological Survey Bulletin* 26, 1-24.

Fedoroff, N., 1997. Clay illuviation in red Mediterranean soils. *Catena* 28, 171–189.

Fedoroff, N., Courty, M-A, Guo. Z., 2010. Palaeosoils and relict soils. In: Stoops G, Marcelino V, Mees F (eds), *Interpretation of Micromorphological Features of Soils and Regoliths*. Elsevier Science, pp. 623-662.

Frechen, M., Neber, A., Tsatskin, A., Boenigk, W., Ronen, A., 2004. Chronology of Pleistocene sedimentary cycles in the Carmel Coastal Plain of Israel**.** *Quaternary International*, 121(1), 41-52.

Gilead, D., Ronen, A., 1977. Acheulian Industries from Evron on the Western Galilee coastal plain al Plain. In: *Eretz-Israel, Archaeological, Historical and Geographical Studies*, vol. 13, Moshe Stekelis Memorial Volume, Israel Exploration Society, Jerusalem, pp.56-86.

Gvirtzman, G., Wieder, M., 2001. Climate of the last 53,000 years in the eastern Mediterranean, based on soil-sequence stratigraphy in the coastal plain of Israel. *Quaternary Science Reviews* 20, 1827-1849.

Koyumdjiski, H., Dan, J., Soriano, S., Nissim, S., 1988. *Selected Soil Profiles of Israel Soils.* Volcani Center, Bet Dagan, 244 pp.

Murray, A., and Wintle, A.G., 2000. Luminescence dating of quartz using an improved single-aliquot regenerative-dose protocol. *Radiation Measurements*, 32: 57–73.

Porat, N., 2007. *Analytical Procedures in the Luminescence Dating Laboratory* (In Hebrew). Geological Survey of Israel. 33 p.

Porat, N., Ronen, A., 2002. Luminescence and ESR Age Determinations of the Lower Paleolithic Site Evron Quarry, Israel. *Advances in ESR Applications,* 18, 123-130.

Porat, N., Wintle, A.G., Ritte, M., 2004. Mode and timing of Kurkar and Hamra formation, central coastal plain. Israel, *Israel Journal of Earth Science* 53, 13-26.

Porat, N., Duller, G.A.T., Roberts, H.M., Wintle A.G., 2009. A simplified SAR protocol for TT-OSL. *Radiation Measurements* 44, 538-542.

Ronen, A., 1991. The lower palaeolithic site Evron-Quarry in western Galilee, Israel. *Sonderveröffentlichungen*, Geologisches Institut der Universität zu Köln 82 (Festschrift Karl Brunnacker), 187-212

Ronen, A., Golik, A., Neber, A., Tsatskin, A**.,** Boenigk, W., Beiles, A., 2005. Pleistocene and Holocene pattern of sand migration along the Mediterranean littoral of Israel, *Israel Journal of Earth Science* 54, 187-198.

Sandler, A., 2009. Pedogenic illite in red-brown Mediterranean soils. *Isr. Soc. Clay Res. Ann. Meet, 2009, Jerusalem, Abstr.,* P. 9.

Sandler, A., Herut, B. 2000. Composition of clays along the continental shelf off Israel: contribution of the Nile versus local sources. *Marine Geology* 167, 339-354

Sandler, A., Almogi-Labin A., Porat, N., 2007. Clays of the Haifa Bay subsurface: high temporal and spatial variability. *Isr. Soc. Clay Res. Ann. Meet, 2007, Volcani Center, Bet Dagan, Abstr.,* P. 4.

Sandler A., Bar Tal A., Fine P., 2009. The impact of irrigation and fertilization on the composition of cultivated soils (in Hebrew). *Isr. Geol Surv. Rep. GSI/33/2009; Isr. Minist. Agric. & Rural Dev., Volcani Center*, 37 p.

Schaetzl, R.J., Anderson, S, 2005. *Soils: Genesis and Geomorphology*. Cambridge University Press.

Singer, A., 2007. *The Soils of Israel.* Springer-Verlag, Berlin, NewYork.

Sivan, D., 1996. Paleogeography of the Galilee coastal plain al plain during the Quaternary. *Report GSI/18/96, Jerusalem, Geological Survey of Israel* (in Hebrew with English summary).

Sivan, D., Porat, N., 2004. Evidence from luminescence for Late Pleistocene formation of calcareous aeolianite (Kurkar) and paleosol (Hamra) in the Carmel Coast, Israel. *Palaeogeography, Palaeoclimatology, Palaeoecology,* 211, 95-106.

Stoops, G., 2003. *Guidelines for Analysis and Description of Soil and Regolith Thin Sections*. Soil Science Society of America, Inc., Madison, Wisconsin USA.

Stoops, G., Marcellino, V., Mees, F. (eds), 2010. *Interpretation of Micromorphological Features of Soils and Regoliths*. Elsevier Science.

Tchernov, E., Kolska Horwitz, L., Ronen, A., Lister, A., 1994. The Faunal Remains from Evron Quaurry in Relation to Other Lower Paleolithic Hominid Sites in the Southern Levant. *Quaternary Research* 42, 328-339.

Tsatskin, A., Gendler, T.S., Heller, F., Ronen, A., 2008. Near-surface paleosols in coastal sands at the outlet of Hadera stream (Israel) in the light of archeology and luminescence chronology. *Journal of Plant Nutrition and Soil Science* 171, 524-532.

Tsatskin, A., Gendler, T.S., Heller, F., Dekman, I., Frey, G.L., 2009. Towards Understanding Paleosols in Southern Levantine Eolianites: Integration of micromorphology, environmental magnetism and mineralogy. *Journal of Mountain Science* 6, 113-124.

Tsatskin, A., Ronen, A., 1999. Micromorphology of a Mousterian paleosol in aeolianites at the site Habonim, Israel. *Catena* 34, 365–384.

Wieder, M., Gvirtzman, G., 1999. Micromorphological indications on the nature of the Late Quaternary Paleosols in the southern coastal plain of Israel, *Catena* 35, 219–237.

Wieder, M., Yaalon, D.H., 1974. Effect of matrix composition on carbonate nodule crystallization. *Geoderma* 11, 95-121.

Wieder, M., Yaalon, D.H., 1982. Micromorphological fabrics and developmental stages of carbonates nodular forms related to soil characteristics, *Geoderma* 28, 203-220

Wintle, A.G. and Murray, A.S., 2006. Review of quartz optically stimulated luminescence characteristics and their relevance in single-aliquot regeneration dating protocols. *Radiation Measurements*, 41, 369-391

Yaalon, D.H., 1997. Soils in the Mediterranean region: what makes them different? *Catena* 28, 157-169.

Yaalon, D.H., Dan, J., 1967. Factors controlling soil formation and distribution in the Mediterranean coastal plain of Israel during the Quarternary. *Quaternary Soils, 7th INQVA Congress, 1965,* Vol. 9, 322-338.

Yaalon, D.H., Kalmar, D., 1978. Dynamics of cracking and swelling clay soils: displacement of skeletal grains, optimum depth of slickensides, and rate of intra-pedonic turbation. *Earth Surface Processes* 3, 31–42.

Zviely, D., Kit, E., Klein, M., 2007. Longshore sand transport estimates along the Mediterranean coast of Israel in the Holocene. *Marine Geology*, 237, 61-73.

Zviely, D., Kit, E., Rosen, B., Galili, E., Klein, M., 2009. Shoreline migration and beach-nearshore sand balance over the last 200 years in Haifa Bay (SE Mediterranean). *Geo-Marr. Lett*. 29, 93-110.

אבנימלך, מ', 1943. לתולדותיו הגיאולוגיים של עמק החוף בנהריה ובסביבתה. ידיעות החברה לחקר ארץ ישראל ועתיקותיה. שנה י' חוב' ב'-ג'.

אלמגור ג', 2005. חוף הים התיכון של ישראל, משרד התשתיות הלאומיות, המכון הגיאולוגי, דו"ח מס' GSI/13/02

דן י', רז צ', 1970. מפת חבורות הקרקע של ישראל (1:250000), משרד החקלאות, מכון וולקני לחקר החקלאות והאגף לשימור קרקע וניקוז.

משרד החקלאות, מפת חבורות קרקע, 1:50,000